The Thesis Committee for Natalie-Nguyen La
Certifies that this is the approved version of the following thesis:

Production Analysis of Oil Production from Unconventional Reservoirs

Using Bottom Hole Pressures Entirely in the Laplace Space

APPROVED BY

SUPERVISING COMMITTEE:

Supervisor: _____

Larry W. Lake

_____

Kishore K. Mohanty

Production Analysis of Oil Production from Unconventional Reservoirs Using Bottom Hole Pressures Entirely in the Laplace Space

by

Natalie-Nguyen La, BS

Thesis

Presented to the Faculty of the Graduate School of

The University of Texas at Austin

in Partial Fulfillment

of the Requirements

for the Degree of

Master of Science in Engineering

The University of Texas at Austin

May 2015

Dedication

I dedicate my thesis to those who have lovingly supported me throughout my life. A special feeling of gratitude to my loving parents, Chi La and Hanh Nguyen whose supports have given me strength to pursue my studies. I want to give special thanks to Bradley Nguyen for being there with me through the good and the bad times, and for your devoted guidance to my career. My thesis is also dedicated to my brother Thang La, sister Thu Pham, nephew Nathan La, and lovely niece Vivian La.

Acknowledgements

Abstract

Production Analysis of Oil Production from Unconventional Reservoirs Using Bottom Hole Pressures Entirely in the Laplace Space

Natalie-Nguyen La, MSE

The University of Texas at Austin, 2015

Supervisor: Larry W. Lake

Laplace transforms are a powerful mathematical tool to solve many problems that describe fluid flow in unconventional reservoirs. However, for the solutions to be useful in applications, for instance history matching, they must be converted from the Laplace space into the real-time domain. A common practice is to numerically invert the transformed Laplace solution. However, we find substantial benefits if the data sets are handled entirely in the Laplace domain, and fitted to models presented in Laplace space rather than in the time domain.

The data set used in this work is oil production rate and bottom hole pressure (BHP) from a liquid-rich shale play in North America, which we study to understand the decline of production from a tight formation produced by a fractured horizontal well. Since the BHP is relatively constant in the long run, a constant BHP solution is appropriate to analyze inflow performance analysis for most wells. However in some cases, as a result of operational changes to some wells, mainly periodic shut-ins, the

production rate experiences isolated pressure build-ups. Both the production rate and BHP are transformed into the Laplace domain and accounted for in the model. Ours is the first analysis that combines rate and BHP entirely in the Laplace domain. There is no need for a Laplace transform inversion.

Two models whose Laplace solutions are readily available are studied side-by-side, a single-compartment model versus a dual-compartment model. We fit the transformed production data of hundreds of wells to the Laplace models. The algorithm to transform data is fairly simple and computationally inexpensive. Since Laplace transformation smoothes the data, the fits are consistently good. Both models yield realistic and similar estimates of ultimate recovery. In most cases the effect of the second compartment in the dual-compartment model can be ignored, i.e., neglecting the fracture-well interaction. The single-compartment model seems adequate for modeling unconventional reservoirs performance.

The knowledge of the reservoir model parameters provides estimation of the drainage volume and forecast future production. One of the main advantages of this novel history matching method is its ability to eliminating noise from data scatter without losing important information. As a result, we can match data more easily. Moreover, real-time solutions to many fluid flow problems in porous media often cannot be obtained analytically but rather via numerical computation. Our current method eliminates the need of inverting to real-time solutions. Additionally, these solutions often assume simple closed forms in Laplace domain even for very complex geometry (higher number of compartments), facilitating the task of history matching.

Table of Contents

List of Tables

List of Figures

Chapter 1: Introduction

Shale formations were traditionally viewed as source rocks and seals, not reservoir rocks. But at the beginning of the 21st century, shales started to be considered as low-porosity and low-permeability (tight) reservoirs. According to Xu (2011), hydraulic fracturing of a shale formations is necessary to stimulate and produce from these unconventional reservoirs economically. Fractured reservoirs have been the object of intensive research in the geologic as well as the engineering fields since the 80's (Aguilera, 1986).

To make investment decisions on these unconventional plays, reservoir engineers must use accurate models to forecast production and estimate reserves. Two classes of analytical models have been developed for forecasting or analyzing production from oil and gas reservoirs with embedded hydraulic fractures (Xu, 2011). The first class involves empirical models that are developed based on the decline curve equations presented by Arps (1945). According to Ogunyomi (2014b), most empirical decline curve methods have two limitations; the model parameters are not functions of reservoir parameters and they may yield unrealistic values of expected ultimate recovery.

The second class requires closed-form mathematical solutions to governing equations that are obtained through solutions to material balances. However, the real-time solutions of the second models often exist in cumbersome forms that require numerical approximations. This thesis presents more simplified analytic well models of the second class that involve transient solutions presented in the Laplace transform domain.

Laplace transforms are a powerful mathematical tool that allows petroleum engineers to obtain solutions to various complex problems that describe the solution of transient flow problems in porous media (Furman, 2003). As a common practice, in history matching, the solutions are converted from the Laplace space into real-time domain and then fitted with the history to find the model parameters. However, we find substantial benefits if the data sets are handled in the Laplace domain, while fitted to models presented in the Laplace space. Why go through all the troubles finding a real-time solution for a history matching problem when the exact solution in the Laplace space exists and is at one's disposal?

In petroleum engineering, field data such as pressure and production rate are measured as discrete data. In this thesis, the method described by Onur and Reynolds (1988) is employed to transform the production data into Laplace space. The transformed data are fitted to the Laplace models, and the model parameters then provide estimation of the expected ultimate recovery from these unconventional reservoirs.

This novel method allows one to analyze production data with virtually any model that describes the physics behind flow in porous media, without going through the challenges to achieve closed-form inversions. Solving differential equations using the Laplace transforms is not new; however, the ability to extracting information from the model in Laplace space is novel. One of the main advantages of this method is its ability to eliminating noise from data scatter without losing important information, because of the integral nature of the Laplace transforms.

Chapter 2: Analytical Models

2.1 Single Compartment Model- Constant Well Flowing Pressure

First we consider is a simplest, linear flow model that prototypes a multi-stage fractured horizontal well for single-phase oil in oil-bearing shale reservoirs. It is therefore appropriate to assume a constant-viscosity and slightly-compressible fluid model. The single compartment system consists of evenly-spaced, transverse hydro-fractures in a rock matrix. The rock matrix has constant properties such as porosity, fluid saturation, and absolute permeability. The geometry of the flow model is represented by Figure 1. The following assumptions are made:

(1) Equally spaced, rectangular planar fractures in a large, rectangular prism rock matrix

(2) No flow outside of the reservoir boundaries

(3) Fluid in the matrix flows linearly in the y-direction towards the fractures

(4) Permeability in the fractures is so high that there is almost no resistance to flow and fluid from the fractures flows with ease towards the wellbore

(5) The centered, fully perforated horizontal well is producing hydrocarbon at a constant bottom hole pressure that is larger the bubble point pressure
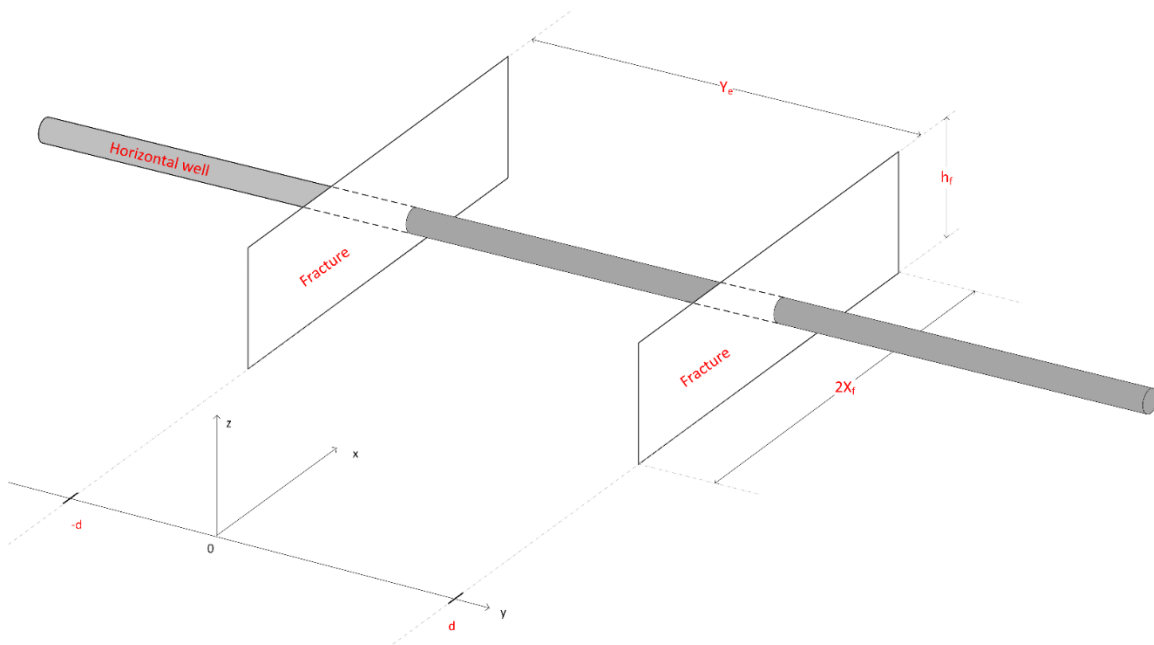
Figure 1:   Schematic of the single compartment model

2.1.2 Matrix Equation

The control volume of the system of interest is bounded in the x-direction by the two parallel fractures, and in the y-direction by the entire length of the fractures. For the defined control volume, the principle of conservation of mass states that as:

Rate of mass IN – Rate of mass OUT = Rate of mass ACCUMULATED   (2.1)

Oil, the only flowing phase, flows linearly in the y-direction from the reservoir matrix to the fracture faces as the contribution of the radial flow to the fracture tip is negligible, and flow from the reservoir rock directly to the wellbore is in the x-direction is insignificant due to ultra-low matrix permeability. Accounting for these factors and taking the limits as Δy approaches 0, and as time t approaches 0, we obtain the following simplified partial differential equation:

4

$$-\frac{\partial(\rho_o u_o)}{\partial y} = \frac{\partial(\phi S_o \rho_o)}{\partial t} \tag{2.2}$$

where ρ_o, S_o are the oil density, oil saturation respectively, and ϕ is the porosity of the reservoir matrix. We need to couple Darcy's law with the mass balance equation to obtain the pressure equation. The superficial velocity of the flowing oil, u_o, is given by:

$$u_o = -\frac{k}{\mu_o}\frac{\partial P}{\partial y} \tag{2.3}$$

where μ_o is the oil viscosity, and k is the absolute permeability of the reservoir matrix. Assuming constant oil saturation, matrix porosity and absolute permeability, by substituting Equation (2.3) into the mass balance equation, we get the pressure diffusivity equation as follows:

$$\frac{k}{\mu_o}\frac{\partial}{\partial y}\left(\frac{\partial P}{\partial y}\right) = \phi S_o\left(\frac{1}{\rho_o}\frac{\partial \rho_o}{\partial P}\right)\frac{\partial P}{\partial t} \tag{2.4}$$

Under relatively constant reservoir temperature, we recognize that $\left(\frac{1}{\rho_o}\frac{\partial \rho_o}{\partial P}\right)_T$ is the isothermal compressibility of oil. Hence, the pressure diffusivity equation can be simplified as:

$$\frac{\partial^2 P}{\partial y^2} = \frac{\phi \mu_o S_o c_o}{k}\frac{\partial P}{\partial t} \tag{2.5}$$

To be more precise, since the pressure equation above describes pressure in the matrix, subscript m for "matrix" is added, and since oil is the only flowing phase, the subscript o for "oil" is dropped for simplification. Total compressibility is calculated by

the formula: $c_t = \sum_{i=1}^{Np} S_i c_i + c_f$ where Np is total number of fluid phases, S and c correspond to saturation and compressibility of phase i respectively. Since the rock formation is considered incompressible hence $c_r = 0$ the total compressibility can be calculated by $c_t = S_o c_o$. Let α_m be the diffusivity coefficient defined by

$$\alpha_m = \left(\frac{k}{\phi \mu c_t}\right)_m \ [=] \frac{length^2}{time}, \text{ then Equation (2.5) can be rewritten as:}$$

$$\frac{\partial^2 P_m}{\partial y^2} = \frac{1}{\alpha_m} \frac{\partial P_m}{\partial t} \qquad (2.6)$$

A second-order partial differential equation is typically defined by an initial condition and two boundary conditions. Initially, pressure is uniform throughout the domain, and equals to the initial pressure P_i of the reservoir:

$$P_m(y,0) = P_i \quad (2.7)$$

The boundary conditions imposed on the system at the fracture faces are constant average pressure $\overline{P}_f$, hence giving rise to the following Dirichlet boundary conditions:

$$P_m(-d,t) = \overline{P}_f$$
$$P_m(+d,t) = \overline{P}_f \qquad (2.8)$$

If the dimensionless variables are defined as follows:

6

$$\begin{cases} P_{Dm} = \dfrac{P_m - \bar{P}_f}{P_i - \bar{P}_f} \\[3mm] y_D = \dfrac{y}{d} = \dfrac{2y}{y_e} \\[3mm] t_D = \dfrac{\alpha_m t}{d^2} \end{cases} \qquad (2.9)$$

then the initial-value problem can be simplified to:

$$\begin{cases} \dfrac{\partial^2 P_{Dm}}{\partial y_D{}^2} = \dfrac{\partial P_{Dm}}{\partial t_D} \\[3mm] P_{Dm}(y_D,0) = 0 \\[2mm] P_{Dm}(-1,t_D) = 0 \\[2mm] P_{Dm}(+1,t_D) = 0 \end{cases} \qquad (2.10)$$

Using the method of Laplace Transform to solve the above partial differential equation, one can arrive at the analytical pressure solution in Laplace space:

$$\hat{P}_{Dm}(y_D,s_D) = \frac{2}{s_D} \frac{\cosh(y_D\sqrt{s_D})}{\cosh(\sqrt{s_D})} \qquad (2.11)$$

where s_D is the dimensionless Laplace variable that corresponds to the dimensionless time variable t_D, correlated to the dimensional Laplace variable by $s_D = \dfrac{d^2 s}{\alpha_m}$. As a convention in this work, Laplace Transformation functions are denoted with hats to distinguish with real-time functions. Next, taking the first-order derivative of $\hat{P}_{Dm}$ with respect to y_D to obtain the dimensionless pressure gradient as:

$$\frac{\partial \hat{P}_{Dm}}{\partial y_D} = \frac{2}{\sqrt{s_D}} \frac{\sinh(y_D\sqrt{s_D})}{\cosh(\sqrt{s_D})} \qquad (2.12)$$

Substituting Darcy's law that gives the fluid flow rate through a porous medium as a function of the pressure gradient, we obtain the following equation:

$$q(t) = -\frac{2A_f k_m}{\mu} \frac{\partial P(y,t)}{\partial y}\bigg|_{y=\pm\frac{L}{2}} \qquad (2.13)$$

The Laplace Transform of the Darcy's equation above gives the Laplace volumetric flow rate as:

$$\hat{q}(s) = -\frac{2A_f k_m}{\mu} \frac{\partial \hat{P}(y,s)}{\partial y}\bigg|_{y=\pm\frac{L}{2}} \qquad (2.14)$$
$$= \frac{4A_f k_m (P_i - \bar{P}_f)}{\mu\sqrt{\alpha_m}\sqrt{s}} \tanh\left(d\sqrt{\frac{s}{\alpha_m}}\right)$$

A_f is the hydraulic fractures fluid contact area, calculated by the relation $A_f = 2x_f h_f$ where x_f is the fracture half-length, and h_f is the fracture thickness, also the pay zone, assuming that the fracture fully penetrates the reservoir. Note that the unit of $\hat{q}(s)$ is $length^3$, which is consistent with the dimensional analysis in Appendix A.4.

For each pair of hydraulic fractures, the Laplace rate- Equation (2.14), a short-term for the Laplace Transform of the volumetric rate solution, can be inverted analytically into the time domain as:

$$q(t) = \frac{8A_f k_m (P_i - \bar{P}_f)}{\mu y_e} \sum_{n=1}^{\infty} e^{\frac{-\pi^2 \alpha_m (2n-1)^2 t}{y_e^2}} \qquad (2.15)$$

If there are $N-1$ parallel hydraulic fractures that position back to back in the direction perpendicular horizontal well, then there are $N-1$ pairs of hydraulic fractures.

8

Using the principle of space superposition, the total volumetric flow rate is the sum of the individual flow rate in each pair of hydraulic fractures:

$$q_T(t) = \frac{8(N-1)A_f k_m (P_i - \bar{P}_f)}{\mu y_e} \sum_{n=1}^{\infty} e^{\frac{-\pi^2 \alpha_m (2n-1)^2 t}{y_e^2}} \qquad (2.16)$$

We recast the Laplace rate and the real-time rate solutions in terms of the lumped model parameters to decrease the number of unknown variables, thus facilitating the task of history matching. Let the following variables be:

$$E = \frac{4(N-1)A_f k_m (P_i - \bar{P}_f)}{\mu \sqrt{\alpha_m}} [=] \frac{L^3}{\sqrt{time}}$$

$$F = \frac{y_e}{2\sqrt{\alpha_m}} [=] \sqrt{time} \qquad (2.17)$$

then our simple lumped-parameter model in either domain becomes:

$$\hat{q}_T(s) = \frac{E}{\sqrt{s}} \tanh\left(F\sqrt{s}\right) \qquad (2.18)$$

$$q_T(t) = \frac{2E}{F} \sum_{n=1}^{\infty} e^{\frac{-\pi^2 (2n-1)^2 t}{4F^2}} \qquad (2.19)$$

The cumulative oil production after an elapsed time t on production is expressed, in terms of the lumped model parameters, as:

$$Q_T(t) = \int_0^t q(\tau)d\tau = \frac{8EF}{\pi^2} \sum_{n=1}^{\infty} \frac{1}{(2n-1)^2}\left(1 - e^{\frac{-\pi^2 (2n-1)^2 t}{4F^2}}\right) \qquad (2.20)$$

On one hand, the real-time analytical solution of the single compartment model involves an infinite series of exponential functions. Since the traditional history matching method requires simple algebraic expressions as reservoir model, the infinite series

9

solution is not a candidate for application. Therefore, one would need an extra step which is to numerically approximate the summation expression in Equation (2.19). On the other hand, the Laplace solution of the same model has a much simpler form, making the fitting of the analytical model to the observed data possible.

2.1.3 An Estimate to the Ultimate Recovery

In this section, we use the theorems involving the limits of the Laplace Transform studied in Appendix B to find the estimated ultimate recovery (EUR) or alternatively, the ultimate recoverable resources (URR). The relation between the volumetric rate and the cumulative produced volume is given by:

$$Np(t) = \int_0^t q(t)dt \qquad (2.21)$$

The EUR can be approximated by the limit of the cumulative production as time approaches infinity:

$$EUR = \lim_{t \to \infty} Np(t) \qquad (2.22)$$

Combining Equations (2.21) & (2.22) with the knowledge of the late-time behavior of the Laplace Transform inversion and the Laplace Transform of an integral, i.e., Equations (A.3) & (A.8) , we arrive at the following relation:

$$EUR = \lim_{t \to \infty} Np(t) = \lim_{s \to 0} \left[s * \hat{N}p(s) - \cancel{Np(0)} \right] = \lim_{s \to 0} \hat{q}(s) \qquad (2.23)$$

which establishes that the ultimate recovery can be approximated by the limit of the Laplace rate solution as s approaches zero, assuming that there is no initial production.

The newly derived relation is then applied to our single-compartment model with constant flowing well pressure, Equation (2.18), to obtain an explicit expression for the EUR:

$$EUR = \frac{2(N-1)A_f dk_m (P_i - \bar{P}_f)}{\mu \alpha_m} \qquad (2.24)$$

Substituting and rearranging the terms, we obtain that the equation derived above is equivalent to $EUR = A_f(N-1)y_e [\phi c_t]_m S_o (P_i - \bar{P}_f)$, where the right side is consistent with the classic definition of the drainage volume. In terms of the lumped model parameters, EUR can be expressed as $E.F$. This is a useful method to obtain the estimated recovery based on the production data and model's fitting parameters. The more data available, the closer this estimate to the true ultimate recovery of the reservoir.

2.1.4 Model Validation

Next, to validate the physical existence of the single compartment model, we are going to reconstruct the fractured tight reservoir through numerical simulation then compare the simulation results with the derived equation for the model. The data produces in this work was generated by CMG simulator from Computer Modeling Group Inc. A 101x1x1 grid system is utilized in the simulator with $\Delta x = 0.5$ ft, $\Delta y = 1000$ ft, and $\Delta z = 10$ ft. The 101st grid, acting as the fracture, contains a vertical well flowing at constant bottom hole pressure of 2000 psi. The grid has a small porosity of 10^{-5} and a high permeability of 10^7 md to ensure constant pressure condition across the fracture. It was found by comparing with the model's real-time analytical solution that the maximum

time-step size of 0.05 day is required to give accurate results. Data specific to the model is shown in Table 1. Schematics of the reservoir simulation model, with color code attributed to permeability, are shown in Figure 2 and 3.

Reservoir grid configuration	101 x 1 x 1
Reservoir size	50.5 ft × 1000 ft × 10 ft
Initial reservoir pressure	5000 psia
Bottom hole pressure	2000 psia
Matrix permeability	10^{-1} md
Matrix porosity	6.5×10^{-2}
Fracture width	0.5 ft
Oil viscosity	2 cp
Oil saturation	1.0
Total compressibility	3.7×10^{-5} psi^{-1}

Table 1:   Reservoir specifications for the validation of the single compartment model
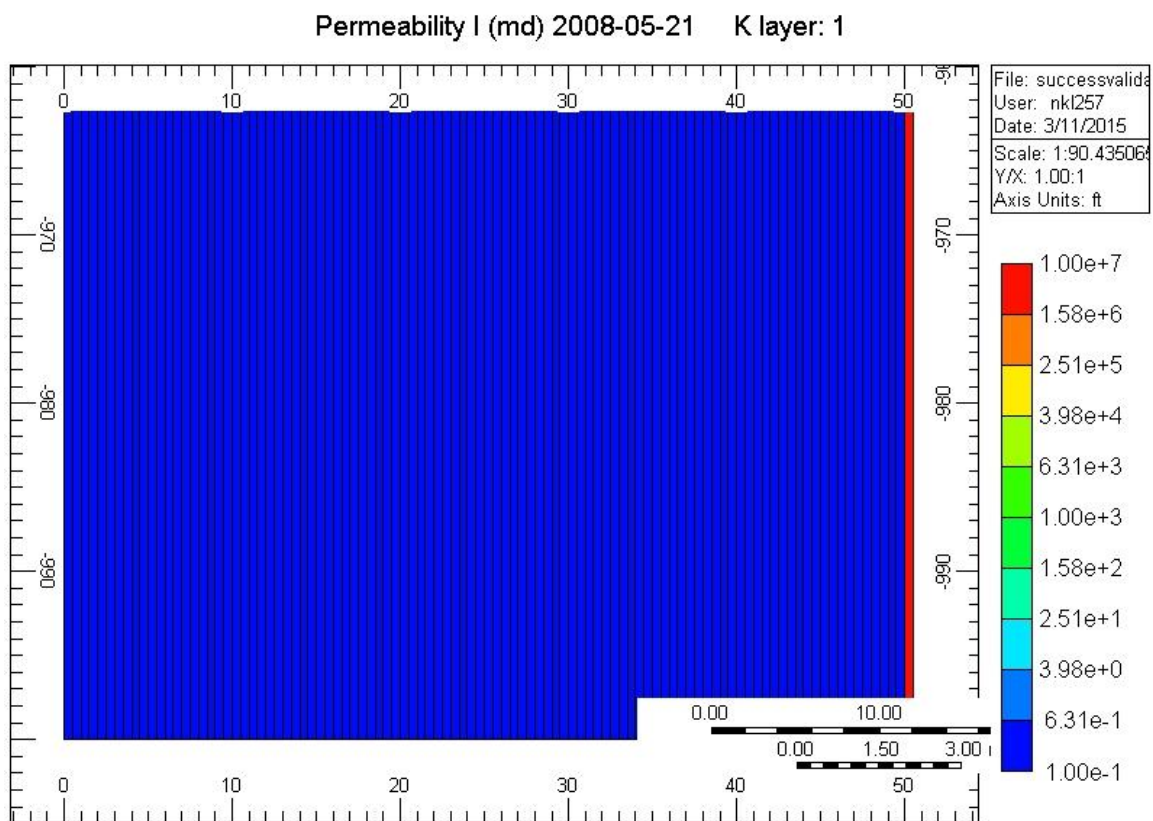
Figure 2. The xy cross-section view of the reservoir.
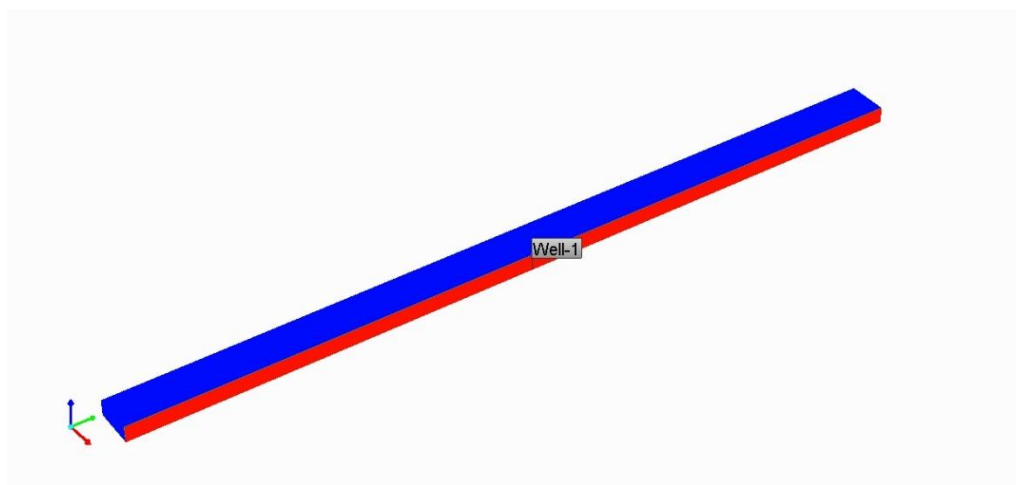
Figure 3: The three dimensional view of the reservoir
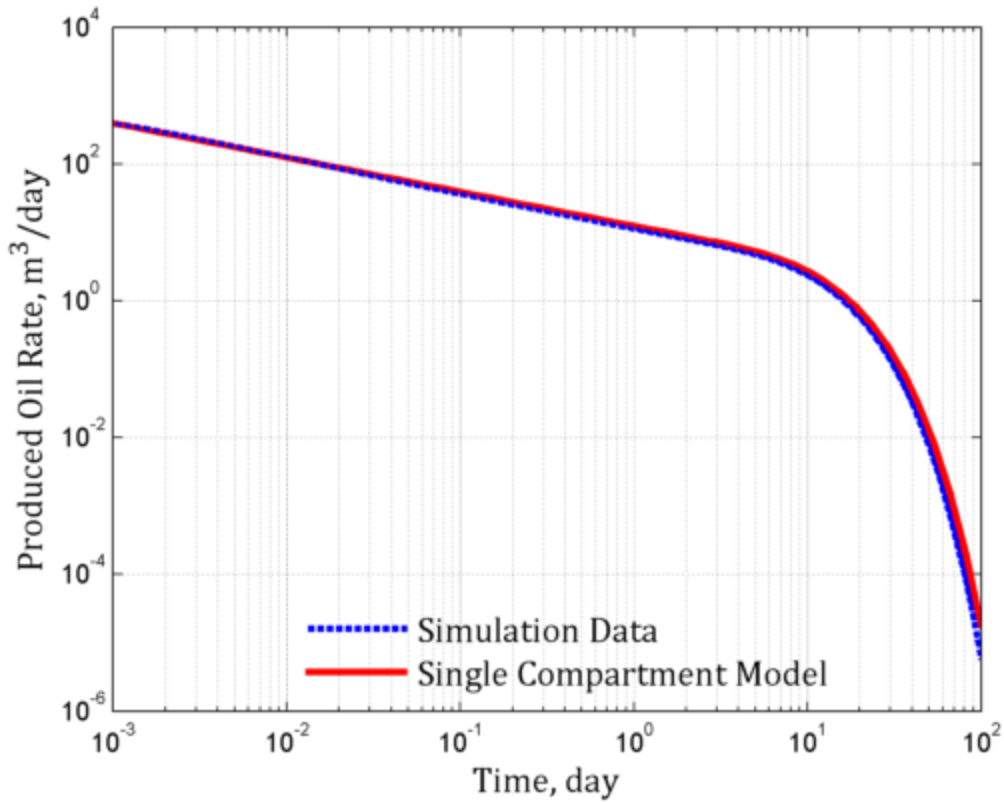
Figure 4:   Comparison between the solutions to the single compartment model and
             simulation results

The comparison between the simulation results and the real-time analytical

solution is shown in Figure 4. We expect to see all the physical meanings underlying in

our model by data produce by CMG, such as:

- A linear flow period with a one-half slope follows, which represents the transient

  flow from the reservoir matrix to the fracture. This flow regime often is the major

  contribution during the life of the well

14

- When flow reaches the external boundary of the reservoir matrix, an exponential decline, also known as the pseudo-steady state flow, is observed (Walsh and Lake, 2003)

It can be observed from Figure 4 that the numerical and analytical results are similar and carry all the flowing regimes. They both exhibit the production signature of the fractured tight reservoirs including the matrix transient linear response initially, and the matrix boundary-dominated flow at later time.

2.2 SINGLE COMPARTMENT MODEL- VARIABLE WELL FLOWING PRESSURE

Oil production wells are intended to be operated at constant bottom hole pressure (BHP) because of the wellhead pressure imposed by constant choke size. Therefore, in most cases, a constant flowing well pressure solution is appropriate to analyze inflow performance analysis (Guo, 2007). The underlying assumption is that the BHP instantaneously drops from the reservoir initial pressure to the constant value determined by the production operations. However, in reality, the BHP often varies during the operational life of the well depending on the shut-in schedule of the production engineers. Furthermore, it would take some time for the pressure to attend equilibrium either when the well, first at initial pressure P_i, is opened and produced or when the well flowing pressure's adjustment occurs Therefore, we wish to extend our simple model to consider variable P_{wf}. Three main assumptions are made

(1) The data that reflect the behavior of the well flowing pressure with respect to time is available.

15

(2) Because of the high fracture permeability which facilitates flow in the fracture, pressure in the fracture P_f propagates quickly to be almost equal to the wellbore pressure P_{wf}; hence, the changes made to the producing well's flowing pressure translate quickly to the same changes to fracture's pressure.

(3) When production resumes once shut in, well flowing pressure is assumed to have built up to reservoir initial pressure (well pressure often reads 0 during shut in).

Most of the derivations in section 2.1.2 remain valid, except for the Dirichlet boundary conditions, which are time-dependent and expressed by:

$$P_m(-d,t) = P_f(t)$$
$$P_m(+d,t) = P_f(t)$$
(2.25)

Using the method of Laplace Transform to solve the above partial differential equation, one can arrive at the analytical volumetric rate solution in Laplace space as:

$$\hat{q}(s) = \frac{4A_f k_m}{\mu\sqrt{\alpha_m}\sqrt{s}}\left(P_i - s\hat{P}_{wf}(s)\right)\tanh\left(\frac{y_e}{2}\sqrt{\frac{s}{\alpha_m}}\right)$$
(2.26)

where $\hat{P}_{wf}(s)$ is the Laplace Transform of the well flowing pressure. If P_{wf} is a constant value then $\hat{P}_{wf}(s) = P_{wf}/s$, and Equation (2.26) is converted to the constant BHP solution. We may compute the transform of the pressure data using the numerical algorithm presented in a later chapter, and substitute that into equation (2.26).

Using the Laplace Transform of time derivative and convolution, the Laplace rate can be inverted analytically into time space as:

16

$$q(t) = -\frac{8A_f k_m}{\mu y_e} \int_0^t \left[\frac{dPwf(\tau)}{d\tau} \sum_{n=1}^{\infty} e^{\frac{-\pi^2 \alpha_m (2n-1)^2 (t-\tau)}{y_e^2}} \right] d\tau \quad (2.27)$$

Since there are $N-1$ pairs of hydraulic fractures, the total volumetric flow rate can be expressed in terms of the individual flow rate in each pair of hydraulic fractures as:

$$q_T(t) = -\frac{8(N-1)A_f k_m}{\mu y_e} \int_0^t \left[\frac{dPwf(\tau)}{d\tau} \sum_{n=1}^{\infty} e^{\frac{-\pi^2 \alpha_m (2n-1)^2 (t-\tau)}{y_e^2}} \right] d\tau \quad (2.28)$$

We recast the Laplace as well as time solutions as a lumped-parameter model to facilitate the task of history matching. Let the following variables be:

$$K = \frac{4(N-1)A_f k_m}{\mu \sqrt{\alpha_m}} [=] \frac{L^3}{Pressure \sqrt{time}}$$

$$F = \frac{y_e}{2\sqrt{\alpha_m}} [=] \sqrt{time} \quad (2.29)$$

then our simple lumped-parameter solution to the model in either domain becomes:

$$\hat{q}_T(s) = \left(\frac{K * P_i}{\sqrt{s}} - K\sqrt{s}\hat{P}_{wf}(s) \right) \tanh\left(F\sqrt{s} \right) \quad (2.30a)$$

$$q_T(t) = -\frac{2K}{F} \int_0^t \left[\frac{dP_{wf}(\tau)}{d\tau} \sum_{n=1}^{\infty} e^{\frac{-\pi^2 (2n-1)^2 (t-\tau)}{4F^2}} \right] d\tau \quad (2.30b)$$

The integral in the last equation can be approximated with a finite sum. Using the midpoint approximation to the integral, and let $x(t) = \sum_{n=1}^{\infty} e^{\frac{-\pi^2 (2n-1)^2 t}{4F^2}}$, Equation (2.30)

becomes

$$q_T(t) = -\frac{2K}{F}\sum_{i=0}^{k-1} x(t - \frac{t_i + t_{i+1}}{2})\left(P_{wf}(t_{i+1}) - P_{wf}(t_i)\right) \qquad (2.31)$$

where k is the number of data points available for the BHP, and $P_{wf}(0) = P_i$.

2.3 DUAL COMPARTMENT MODEL

2.3.1 Introduction

This section considers fluid transport in an idealized system consisting of slabs of saturated rock-matrix separated by equally spaced, planar fractures (Barker 1980). Since the production data of interest is collected from oil-bearing shale reservoirs, it is appropriate to assume a constant-viscosity and constant-compressibility fluid model. The dual compartment system consists of a bounded rectangular reservoir with matrix blocks draining into adjoining fractures and subsequently to a horizontal well in the center (Bello, 2009). The fracture volume is significant and flow in the fractures contributes to the overall flow characteristics, differentiating this model from the single compartment model. The two porous media, fracture and matrix, have different but relatively constant properties such as porosity, and absolute permeability. The geometry of the flow model is presented in Figure 5 with the following assumptions (Barker 1980):

(1) Identical slabs of matrix material separated by equally spaced, planar fractures

(2) There is no pressure gradient across the fractures

(3) Fluid in the matrix blocks flows dominantly in the y-direction towards fractures, and fluid from the fractures flows in the x-direction towards the wellbore

(4) The centered, fully perforated horizontal well is producing hydrocarbon at

constant bottom-hole pressure
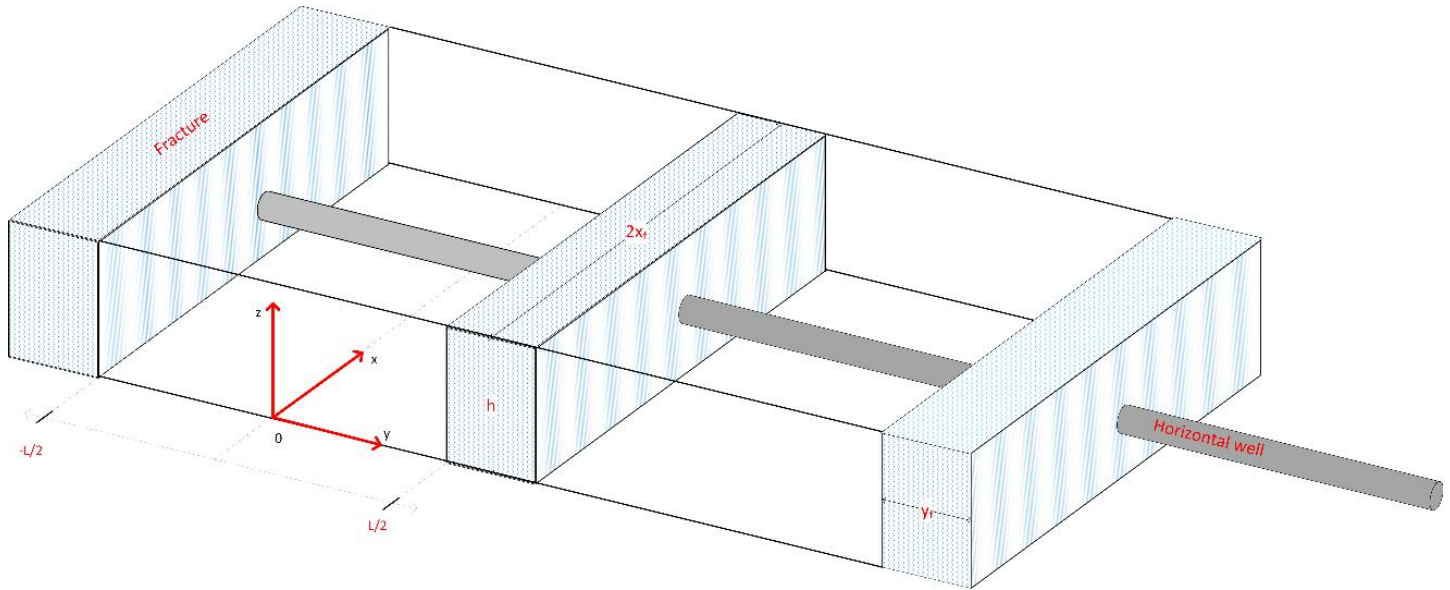
Figure 5:   A schematic of the double compartment model

2.3.2 Matrix Equation

The one-dimensional, linear diffusion pressure equation in the matrix, derived in

great details from the mass balance equation in section 3.1, is summarized as:

$$\frac{\partial^2 P_m}{\partial y^2} = \frac{1}{\alpha_m} \frac{\partial P_m}{\partial t} \qquad (2.32)$$

where α_m is the diffusivity coefficient of matrix, defined by $\alpha_m = \left(\frac{k}{\phi \mu c_t} \right)_m$.

Initially, the pressure in the matrix is constant everywhere, and equals to the

initial pressure P_i of the reservoir:

19

$$P_m(y,0) = P_i \quad (2.33)$$

The boundary conditions imposed on the partial differential equation assume no-flow boundary in the y-direction away from the fracture, while keeping the pressure at the fracture and matrix interface constant. This pressure P_f is also the pressure everywhere in the fracture as fracture permeability is high.

$$\frac{\partial P_m}{\partial y}(0,t) = 0$$

$$\quad (2.34)$$

$$P_m(\frac{L}{2}, t_D) = P_f$$

The following dimensionless variables are defined as:

$$\begin{cases} P_{Dm} = \dfrac{P_i - P_m}{P_i - P_{wf}} \\[2mm] P_{Df} = \dfrac{P_i - P_f}{P_i - P_{wf}} \\[2mm] y_D = \dfrac{2y}{L} \\[2mm] x_D = \dfrac{x}{x_f} \\[2mm] t_D = \dfrac{k_f t}{\mu x_f^2 S_o \left([\phi c_t]_m + [\phi c_t]_f \right)} = \dfrac{\alpha_f \omega t}{x_f^2} \end{cases} \quad (2.35)$$

The storativity ratio of the fracture, denoted ω, is defined as: $\omega = \dfrac{[\phi c_t]_f}{[\phi c_t]_m + [\phi c_t]_f}$,

and the interporosity flow parameter, denoted λ, as: $\lambda = 12 \dfrac{x_f^2}{L^2} \dfrac{k_m}{k_f}$. The initial-value problem of the matrix equation is rewritten as:

$$\begin{cases} \dfrac{\partial^2 P_{Dm}}{\partial y_D{}^2} = \dfrac{3}{\lambda}(1-\omega)\dfrac{\partial P_{Dm}}{\partial t_D} \\[2mm] P_{Dm}(y_D,0) = 0 \\[2mm] P_{Dm}(1,t_D) = P_{Df}(y_D,t_D) \\[2mm] \dfrac{\partial P_{Dm}}{\partial y_D}(0,t_D) = 0 \end{cases} \qquad (2.36)$$

Next, we are going to integrate the solution to the above partial differential problem of the matrix flow to the diffusivity equation for the fracture flow, which is presented in the next section, to arrive at the final solution for the dual compartment model.

2.3.3 Fracture Equation

The one-dimensional, linear diffusion pressure equation for flow from the fracture into the wellbore is written as:

$$\frac{\partial^2 P_f}{\partial x^2} = \frac{1}{\alpha_f}\frac{\partial P_f}{\partial t} - \frac{k_m}{k_f}\frac{2}{L}\frac{\partial P_m}{\partial y}\bigg|_{y=\frac{L}{2}} \qquad (2.37)$$

where α_f is the diffusivity coefficient of the fracture, defined as $\alpha_f = \left(\dfrac{k}{\phi\mu c_t}\right)_f$. The additional term on the right-hand side is the source term, which describes the fluid flow from the matrix into the fracture at their interfaces.

Initially, the pressure in the fracture is the same everywhere, and equals to the initial pressure P_i of the reservoir:

$$P_f(x,0) = P_i \qquad (2.38)$$

The boundary conditions imposed on the partial differential equation assume no-flow boundary in the x-direction, far away from the wellbore, while fixing pressure at the sand face to equal the constant bottom hole pressure:

$$\frac{\partial P_f}{\partial x}(0,t) = 0$$
$$P_f(x_f, t_D) = P_{wf}$$

(2.39)

If the dimensionless variables are defined as in (2.35) then the initial-value problem of fracture equation is rewritten as:

$$\begin{cases} \dfrac{\partial^2 P_{Df}}{\partial x_D{}^2} = \omega \dfrac{\partial P_{Df}}{\partial t_D} - \dfrac{\lambda}{3} \dfrac{\partial P_{Dm}}{\partial y_D}\bigg|_{y_D=1} \\[2mm] P_{Df}(x_D, 0) = 0 \\[1mm] P_{Df}(1, t_D) = 1 \\[1mm] \dfrac{\partial P_{Df}}{\partial x_D}(0, t_D) = 0 \end{cases}$$

(2.40)

Using the method of Laplace Transform to solve systems of Equations (2.36) and (2.40), one can arrive at the analytical pressure solution in Laplace space:

$$\hat{P}_{Df} = \frac{1}{s_D} \frac{\cosh(y\sqrt{s_D f(s_D)})}{\cosh(\sqrt{s_D f(s_D)})}$$

(2.41)

where $f(s_D) = \omega + \sqrt{\dfrac{\lambda(1-\omega)}{3 s_D}} \tanh\sqrt{\dfrac{3(1-\omega)s_D}{\lambda}}$

and s_D is the dimensionless Laplace variable that corresponds to the dimensionless time variable t_D, defined as $s_D = \dfrac{x_f{}^2 s}{\alpha_f \omega}$.

22

Substituting Darcy's law that gives the fluid flow rate through a porous medium as a function of the pressure gradient, we obtain the following equation for the flow rate into one hydraulic fracture as:

$$q_f(t) = -\frac{2A_r k_f}{\mu} \frac{\partial P_f}{\partial x}\bigg|_{y=\frac{L}{2}} \qquad (2.42)$$

where A_r is the y-z cross-sectional area of the fracture, and is calculated by the relation $A_r = y_f h$.

The Laplace Transform of the Darcy's equation above gives the Laplace volumetric flow rate as:

$$\hat{q}_f(s) = -\frac{2A_r k_f}{\mu} \frac{\partial \hat{P}_f}{\partial x}\bigg|_{y=\frac{L}{2}}$$
$$= \frac{2A_r x_f k_f (P_i - P_{wf})}{\mu \alpha_f \omega} \sqrt{\frac{f(s_D)}{s_D}} \tanh(\sqrt{s_D f(s_D)}) \qquad (2.43)$$

If there are N parallel hydraulic fractures that position back to back in the direction perpendicular horizontal well, then using the principle of space superposition, the total volumetric flow rate is the sum of the individual flow rate in each hydraulic fracture:

$$\hat{q}_{fT}(s) = \frac{2NA_r x_f k_f (P_i - P_{wf})}{\mu \alpha_f \omega} \sqrt{\frac{f(s_D)}{s_D}} \tanh(\sqrt{s_D f(s_D)}) \qquad (2.44)$$

Unit of $\hat{q}_f(s)$ or $\hat{q}_{fT}(s)$ is $length^3$, which is consistent with the dimensional analysis. The analytical inversion of the above Laplace rate solution is complicated, and

23

requires numerical approximation. The Laplace solution to any number of compartments exists in similar form as Equation (2.44), and the more compartments being modeled, the more nested the solution becomes.

The two models proposed in this thesis are one of the simplest models of the reservoir engineering problems; however both real-time solutions require cumbersome mathematical estimation for history matching applications. Now let us take a step back, since our study focuses on extracting important reservoir characteristics from the solution in the Laplace space, the agonizing step of inverting the Laplace solution step is no longer essential.

Next, we recast the Laplace as well as the real-time solutions in terms of the model lumped parameters to reduce the number of unknown, thus facilitating the task of history matching. Let the following variables be:

$$a = \frac{2NA_r x_f k_f (P_i - P_{wf})}{\mu \alpha_f \omega}[=]length^3$$

$$c = \frac{x_f^2}{\alpha_f \omega}[=]time$$

$$(2.45)$$

then our simple lumped-parameter model in Laplace domain becomes:

$$\hat{q}_{fT}(s) = a\sqrt{\frac{\omega}{cs} + \left(\frac{1}{cs}\right)^{3/2}} \sqrt{\frac{\lambda(1-\omega)}{3}} \tanh\sqrt{\frac{3(1-\omega)cs}{\lambda}} \tanh\left(\sqrt{\omega cs + \sqrt{\frac{\lambda(1-\omega)cs}{3}}} \tanh\sqrt{\frac{3(1-\omega)cs}{\lambda}}\right)(2.46)$$

The solution to the cumulative volume in the Laplace space can be expressed in terms of the Laplace rate as:

$$\hat{Q}_T(s) = \frac{\hat{q}_{fT}(s)}{s} \qquad (2.47)$$

24

A problem with using the solution presented in (2.46) is that it cannot be inverted back into the real-time space to obtain a closed-form analytical solution (Ogunyomi, 2014b). Hence, the Gaver-Stehfest algorithm for numerical inversion of the Laplace Transform, presented in appendix B, is employed to evaluate the function $q_{fT}(t)$ and $Q_T(t)$

2.3.4 An Estimate of the Ultimate Recovery

In this section, we are going to apply the relation derived in Equation (2.23) to the dual compartment model to obtain an explicit expression for the EUR:

$$EUR = \frac{NA_r x_f k_f (P_i - P_{wf})}{\mu \alpha_f \omega} \quad (2.48)$$

In terms of the model parameters, EUR can be expressed as $EUR = a$. This is a useful method to obtain the estimated recovery based on the production data and model's fitting parameters. The more data available, the closer this estimate to the true ultimate recovery of the reservoir.

2.3.5 Model Validation

Next, we are going to validate the dual compartment model through numerical simulation. A $101 \times 1 \times 1$ grid system is used in the simulator with $\Delta x = 1$ ft, $\Delta y = 100$ ft, and $\Delta z = 100$ ft. The first 50 grids carry the matrix properties, and the next 50 grids constitute the stimulated reservoir volume (SRV). The 101st grid, acting as the fracture, contains the well at constant bottom hole pressure of 2000 psi, and is assigned a small porosity of 10^{-7} and a high permeability of 10^7 md to ensure constant pressure condition

across the fracture. It was found by comparing with the analytical solution that the maximum time-step size of 0.05 day is required to give accurate results. Data specific to the model is shown in Table 2. Schematics of the reservoir simulation model, with color code attributed to permeability, are shown in Figure 6 and 7.

Reservoir grid configuration	$101 \times 1 \text{ x} \times 1$
Grid size	$1 \times 100 \text{ ft} \times 100 \text{ ft}$
Reservoir size	$101 \text{ ft.} \times 100 \text{ ft} \times 100 \text{ ft}$
Initial reservoir pressure	5000 psia
Bottom-hole pressure	2000 psia
Matrix permeability	8×10^{-4} md
Matrix porosity	10^{-5}
SRV permeability	10^2 md
SRV porosity	10^{-5}
Fracture width	1 ft
Oil viscosity	2 cp
Oil saturation	1.0
Total compressibility	3.7×10^{-5} psi^{-1}

Table 2:   Reservoir specifications for the validation of the dual compartment model
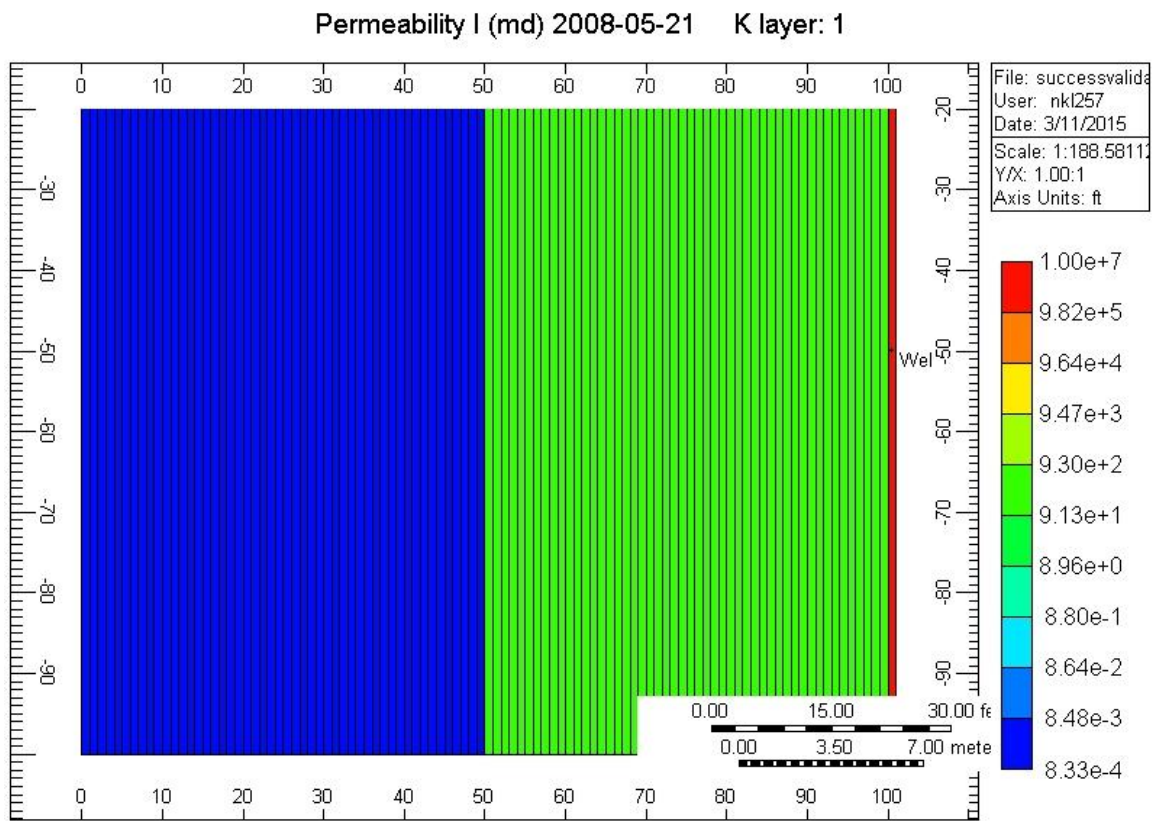
Figure 6:   The xy cross-section view of the reservoir
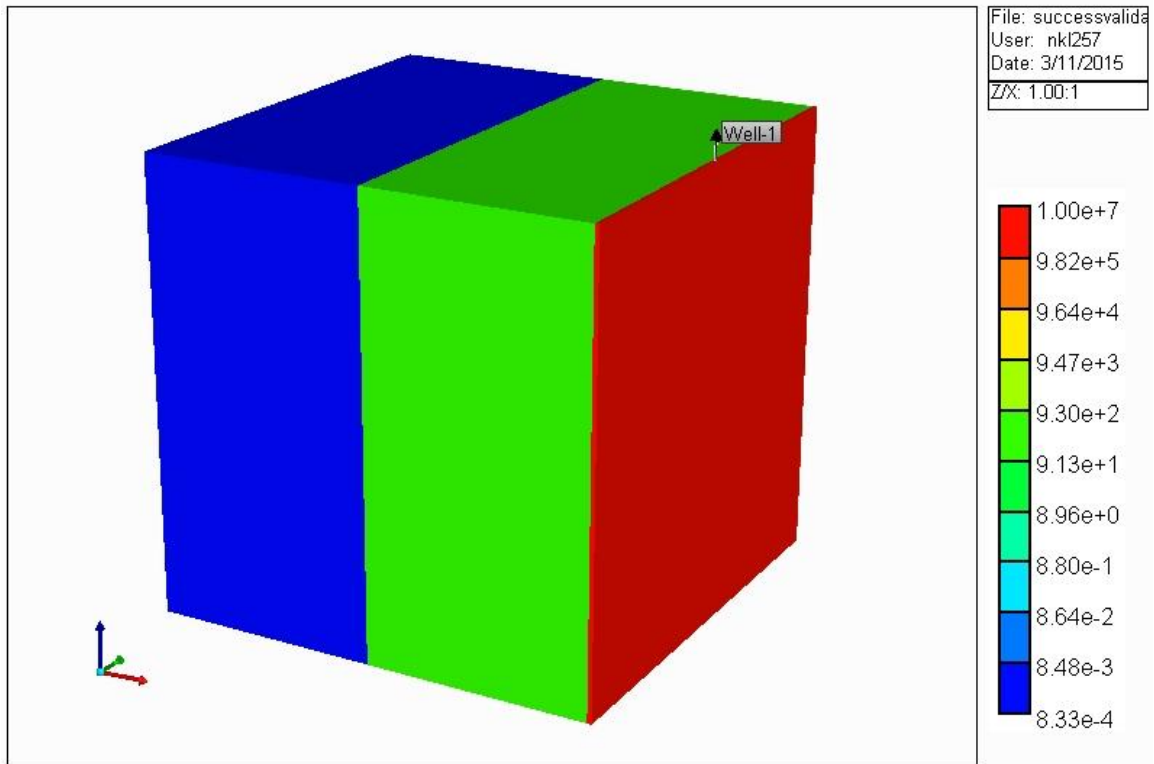
Figure 7:   The three-dimensional view of the reservoir
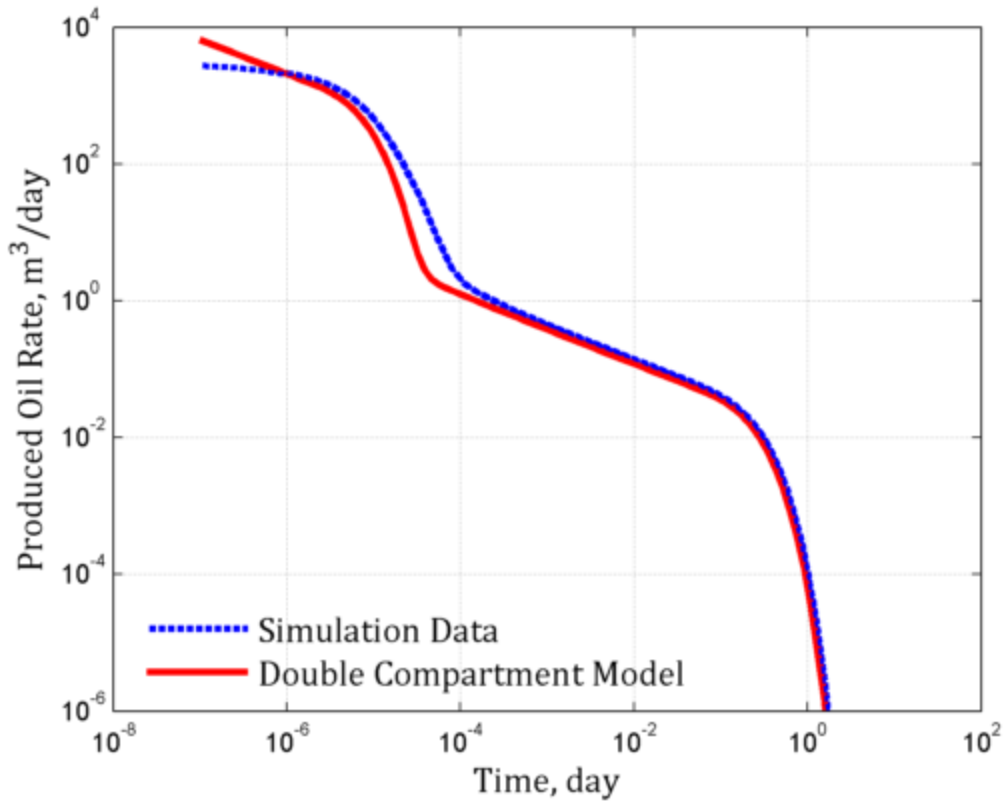
Figure 8:   Comparison between the solutions to the double compartment model and
             simulation results

The results from the numerical simulation is shown in Figure 8. It can be

observed from this figure that the numerical and analytical results show a fairly good

match. As expected from the dual compartment model, both plots display two timescales.

The physical meaning of this characteristic can be explained as follows (Ogunyomi,

2014b):

- At the start of production, flow is predominantly linear with a one-half slope,
  which represents transient flow from the SRV

- When flow reaches the SRV boundary, an exponential decline follows

29

- Another linear flow period with a one-half slope picks up, which represent transient flow from the reservoir matrix to the fracture. This flow regime often is the major contribution during the life of the well

- When flow reaches the external boundary of the reservoir matrix, another exponential decline, also known as the pseudo-steady state flow, is observed (Walsh and Lake, 2003)

The second timescale, which includes the matrix transient then matrix boundary-dominated flows, shows better fit than the first timescale. The plateau period observed in the first timescale of the simulation data is as a result of the combination of wellbore storage and fracture skin, a factor which the dual compartment model does not account for (Stewart, 2011), however can be easily be integrated when needed.

Chapter 3: Numerical Laplace Transform of Discrete Data

The Laplace Transform, named after the French mathematician Pierre-Simon Laplace, is a method for solving problems that arise in several areas of mathematical analysis. Of particular importance is its ability to solve partial differential equations, which continually emerge in engineering problems in general and the problem of fluid-flow in permeable media in particular (Bellman, 1984).

The Laplace Transform of a function $f(t)$, for all real non-negative values of t, is defined by:

$$\mathcal{L}\{f(t)\} = F(s) = \int_{t=0}^{t=\infty} e^{-st} f(t) dt \qquad (3.1)$$

where t is the time variable with unit of time, and s is the complex frequency variable with unit of inverse of time, i.e., time^{-1}. The Laplace Transform is a mapping from points in the time domain to points in the frequency domain. For the operation of the Laplace transformation to make sense, the image of $f(t)$, denoted $F(s)$, requires that the improper integral on the right side must converge. The variables of interest in reservoir engineering are often flow rate and pressure, and they generally display declining behavior in the infinite time range and thus constitute suitable functions $f(t)$.

The novel idea behind this work is handling data and model fitting in the Laplace space to obtain useful reservoir parameters that can be applied to validate the fit in the real-time domain or to estimate the drainage volume; hence most of this chapter focuses on introducing and optimizing the mathematical tools that revolve around this work.

31

Data obtained from the field exist in the time domain. The available tool that enables the conversion of such data to the Laplace space is a critical requirement for the success of our method. Fortunately, Onur and Reynolds (1998) proposed algorithms to accurately transformed sampled data into Laplace space. Because of the nature of the Laplace Transform, which requires knowledge of the function over a semi-infinite time interval from 0 to infinity, a complete algorithm to compute the Laplace Transform of sampled data is comprised of three parts: early-time interpolation, discrete-data interpolation, and late-time extrapolation (Onur 1998). The Laplace Transform of sampled data, represented by some underlying function $f(t)$, is thus calculated by

$$\hat{f}(s) = \int_0^{t_1} f(t)e^{-st}dt + \int_{t_1}^{t_N} f(t)e^{-st}dt + \int_{t_N}^{\infty} f(t)e^{-st}dt \qquad (3.2)$$

Let I_1, I_2, I_3 be the intervals from left to right respectively, then I_1 represents the early-time interpolation, I_2 the discrete-data interpolation, and I_3 the late-time extrapolation. To accommodate the noise of the sampled data, the representative function could be piecewise linear, piecewise quadratic, or log-linear. Different functions have different complexities that require special care while handling. The following sections serve as guidelines for transforming data that display the behaviors similar to as described below.

3.1 EARLY-TIME INTERPOLATION

A log-linear functional representation provides accurate early-time interpolation of data (Onur, 1998). Let $f(t) = \alpha t^{\beta}$ then the first interval can be written as:

$$I_1 = \int_0^{t_1} f(t) e^{-st} dt$$

$$= \int_0^{t_1} \alpha t^\beta e^{-st} dt$$

$$= \int_0^\infty \alpha t^\beta e^{-st} dt - \int_{t_1}^\infty \alpha t^\beta e^{-st} dt \qquad (3.3)$$

$$= \int_0^\infty \frac{\alpha}{s^{\beta+1}} (st)^{(\beta+1)-1} e^{-st} d(st) - \int_{t_1}^\infty \frac{\alpha}{s^{\beta+1}} (st)^{(\beta+1)-1} e^{-st} d(st)$$

$$= \frac{\alpha}{s^{\beta+1}} \left[\int_0^\infty (st)^{(\beta+1)-1} e^{-st} s\, dt - \int_{t_1}^\infty (st)^{(\beta+1)-1} e^{-st} s\, dt \right]$$

$$= \frac{\alpha}{s^{\beta+1}} \left[\Gamma(\beta+1) - \Gamma(\beta+1, st_1) \right]$$

where the gamma function, denoted $\Gamma(t)$, is defined as: $\Gamma(t) = \int_0^\infty x^{t-1} e^{-x} dx$, and the

incomplete gamma function, denoted $\Gamma(t,u)$, as: $\Gamma(t,u) = \int_u^\infty x^{t-1} e^{-x}$ for $t > 0$. The

coefficients α and β of the early-time interpolation, determined from the first few data

points, are given by the formulas: $\beta = \dfrac{\ln(f_2 / f_1)}{\ln(t_2 / t_1)}$; $\alpha = \dfrac{f_1}{t_1^\beta}$, where f_i for $i = 1, 2, ..., N$

denotes the ith data point in the sample.

3.2 DISCRETE-DATA INTERPOLATION

Piecewise-linear functional representation is widely used in discrete-data

interpolation because of to its simplicity. Suppose that each pair of data points can be

represented by a linear function, i.e., $f(t) = f_i + m_i(t - t_i)$ for the interval $t_i < t < t_{i+1}$ where

m_i is the slope of the linear interpolation, given by $m_i = \dfrac{f_{i+1} - f_i}{t_{i+1} - t_i}$, then the integral I_2 can

be written as:

$$
\begin{aligned}
I_2 &= \int_{t_1}^{t_N} f(t) e^{-st} dt \\
&= \sum_{i=1}^{N-1} \int_{t_i}^{t_{i+1}} f(t) e^{-st} dt \\
&= \sum_{i=1}^{N-1} \int_{t_i}^{t_{i+1}} \left[f_i + m_i (t - t_i) \right] e^{-st} dt \\
&= \sum_{i=1}^{N-1} \left[\frac{f e^{-st}}{-s} \Big|_{t_i}^{t_{i+1}} - \frac{m_i e^{-st}}{s^2} \Big|_{t_i}^{t_{i+1}} \right] \\
&= \sum_{i=1}^{N-1} \left[\frac{f_i e^{-st_i}}{s} + \frac{m_i (e^{-st_i} - e^{-st_{i+1}})}{s^2} - \frac{f_{i+1} e^{-st_{i+1}}}{s} \right]
\end{aligned}
\qquad (3.4)
$$

For more accuracy, high-order, piecewise-quadratic functions may be used to interpolate between subintervals. Suppose that each subinterval $t_{2i-1} < t < t_{2i+1}$ can be represented by a piecewise Lagrange quadratic function, i.e., $f(t) = f_{2i-1} L_{2i-1} + f_{2i} L_{2i} + f_{2i+1} L_{2i+1}$, where L_k is the second degree Lagrange interpolating polynomial, given by $L_k = \prod_{i=k-1, i \neq k}^{k+1} \dfrac{(t - t_i)}{(t_k - t_i)}$ (Burden 2011), then the interval I_2 can be expressed as:

$$I_2 = \int_{t_1}^{t_N} f(t)e^{-st}\,dt$$

$$= \sum_{i=1}^{M} \int_{t_{2i-1}}^{t_{2i+1}} f(t)e^{-st}\,dt$$

$$= \sum_{i=1}^{M} \int_{t_{2i-1}}^{t_{2i+1}} \left(f_{2i-1}L_{2i-1} + f_{2i}L_{2i} + f_{2i+1}L_{2i+1} \right)e^{-st}\,dt$$

$$= \sum_{i=1}^{M} \int_{t_{2i-1}}^{t_{2i+1}} \left(f_{2i-1}\frac{(t-t_{2i})(t-t_{2i+1})}{(t_{2i-1}-t_{2i})(t_{2i-1}-t_{2i+1})} + f_{2i}\frac{(t-t_{2i-1})(t-t_{2i+1})}{(t_{2i}-t_{2i-1})(t_{2i}-t_{2i+1})} + f_{2i+1}\frac{(t-t_{2i-1})(t-t_{2i})}{(t_{2i+1}-t_{2i-1})(t_{2i+1}-t_{2i})} \right)e^{-st}\,dt$$

$$= \sum_{i=1}^{M} \frac{1}{s}\left(e^{-st_{2i-1}}f_{2i-1} - e^{-st_{2i+1}}f_{2i+1} \right) + \frac{1}{s^2}\begin{bmatrix} a_i\left(e^{-st_{2i-1}} - e^{-st_{2i+1}}\right) \\ +b_i\left(e^{-st_{2i-1}} + e^{-st_{2i+1}}\right) \\ -c_i\left(e^{-st_{2i-1}} + e^{-st_{2i+1}}\right) \end{bmatrix} + \frac{2}{s^3}\left(l_{2i-1} + m_{2i} + r_{2i+1}\right)\left(e^{-st_{2i-1}} - e^{-st_{2i+1}}\right)$$

(3.5)

where M must be an odd number, given by $\dfrac{\#\ of\ data\ points - 1}{2}$, and

$$a_i = \frac{f_{2i+1} - f_{2i-1}}{t_{2i+1} - t_{2i-1}}; b_i = \frac{f_{2i} - f_{2i-1}}{t_{2i} - t_{2i-1}}; c_i = \frac{f_{2i+1} - f_{2i}}{t_{2i+1} - t_{2i}}$$

$$l_{2i-1} = \frac{f_{2i-1}}{(t_{2i-1} - t_{2i})(t_{2i-1} - t_{2i+1})}; r_{2i+1} = \frac{f_{2i+1}}{(t_{2i+1} - t_{2i-1})(t_{2i+1} - t_{2i})}; m_{2i} = \frac{f_{2i}}{(t_{2i} - t_{2i-1})(t_{2i} - t_{2i+1})}$$

3.3 LATE-TIME EXTRAPOLATION

To obtain an accurate late-time extrapolation, we require some knowledge of the functional behavior of the data as time goes to infinity. Here, we are interested in extrapolating the producing rate of a well, which often display an exponential decline type of behavior at late time during which the effect of the flow boundary is felt. Hence, suppose that $f(t) = \kappa e^{-\gamma t}$ where $\gamma = -\dfrac{\ln(f_N/f_{N-1})}{t_N - t_{N-1}}$ and $\kappa = \dfrac{f_N}{e^{-\gamma t_N}}$ then the last interval I_3

, can be written as:

$$I_3 = \int_{t_N}^{\infty} f(t)e^{-st}dt$$

$$= \int_{t_N}^{\infty} \kappa e^{-\gamma t}e^{-st}dt$$

$$= \int_{t_N}^{\infty} \kappa e^{-(\gamma+s)t}dt \qquad (3.6)$$

$$= \frac{\kappa}{-(\gamma+s)}e^{-(\gamma+s)t}\Big|_{t_N}^{\infty}$$

$$= \frac{\kappa}{(\gamma+s)}e^{-(\gamma+s)t_N}$$

3.4 A COMPLETE ALGORITHM

Generally, combinations of different functional representations can give different algorithms to transform data into the Laplace domain. The works presented in this thesis are done using an algorithm that is formulated based on a log-linear early-time interpolation, a piecewise-linear discrete data-interpolation, and an exponential late-time extrapolation. It is thus formulated as:

$$F(s) = \frac{\alpha}{s^{\beta+1}}\big[\Gamma(\beta+1) - \Gamma(\beta+1, st_1)\big] + \frac{\kappa}{(\gamma+s)}e^{-(\gamma+s)t_N}$$

$$+ \sum_{i=1}^{M}\frac{1}{s}\left(e^{-st_{2i-1}}f_{2i-1} - e^{-st_{2i+1}}f_{2i+1}\right) + \frac{1}{s^2}\begin{bmatrix} a_i\left(e^{-st_{2i-1}} - e^{-st_{2i+1}}\right) \\ +b_i\left(e^{-st_{2i-1}} + e^{-st_{2i+1}}\right) \\ -c_i\left(e^{-st_{2i-1}} + e^{-st_{2i+1}}\right) \end{bmatrix} + \frac{2}{s^3}\left(l_{2i-1} + m_{2i} + r_{2i+1}\right)\left(e^{-st_{2i-1}} - e^{-st_{2i+1}}\right)$$

(3.7) where the interpolating/extrapolating coefficients are defined in the section 3.2.

3.5 TEST FUNCTION

When fitting data, not only the best fit but also the uniqueness of the fit must be determined to understand the confidence one can have in the estimates (Hines et al, 2014). This section validates the accuracy of the numerical transform of data into the

Laplace space and the uniqueness of the estimated model parameters. The uniqueness of the fit is met if modification of the starting points and the upper/lower bounds results in insignificant changes in the best-fit model parameters. Two test functions that correspond to the solutions of the two models developed in this thesis are studied. The method is robust if the Laplace transformation of the discrete data generated from the function $f(t)$ using the algorithm provided in section 3.4 results in data in the Laplace domain that match the Laplace Transform of $f(t)$, denoted $F(s)$.

3.5.1 Test function #1

The first test function involves the solution to the constant flowing pressure (BHP) single compartment linear flow model derived in section 2.1. Thus, test function #1 has the following forms in the Laplace and the time domains, respectively:

$$F(s) = \frac{A}{\sqrt{s}} \tanh\left(B\sqrt{s}\right)$$

$$f(t) = \frac{2A}{B} \sum_{n=1}^{\infty} e^{\frac{-\pi^2 (2n-1)^2 t}{4B^2}}$$

(3.8)

where A and B are arbitrarily chosen to be 1.000 and 1.000 respectively. The variables s and t are assumed dimensionless in this particular example. Figure 9 presents the log-log graph of $f(t)$ versus t.
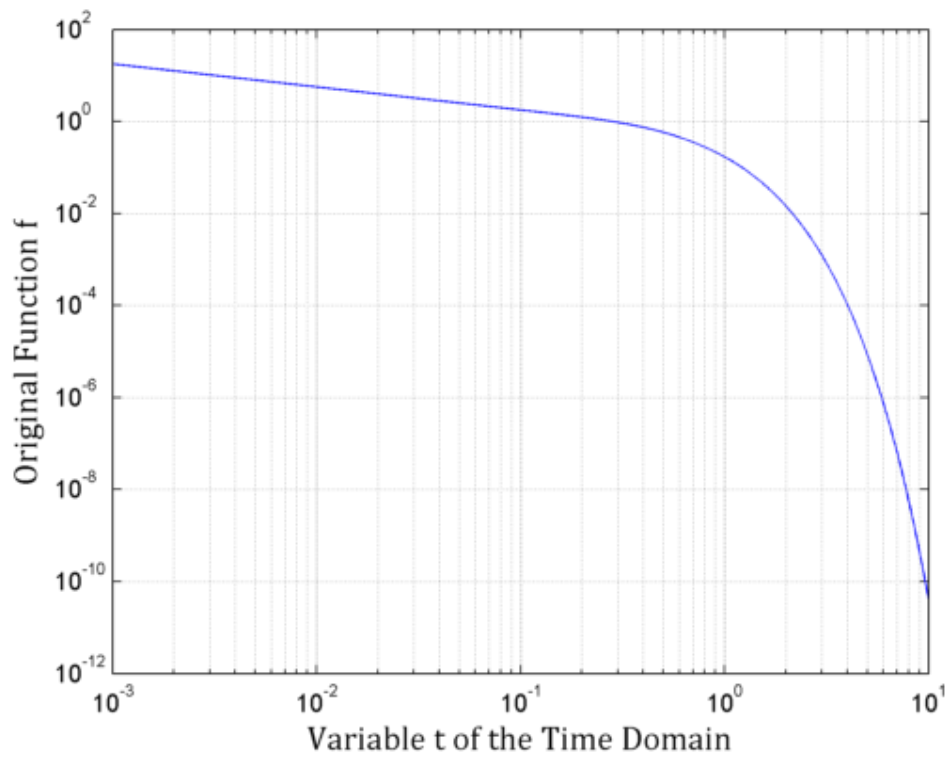
Figure 9:   Function $f(t)$ evaluated over a large range of variable t

In Figure 10, the forward Laplace Transform of the function $f(t)$, in other words $F(s)$, and the numerical Laplace Transform of the data generated from the original function $f(t)$ are plotted against the variable s of the Laplace domain.

Figure 10:   The comparison between $F(s)$ and the numerical Laplace transform of the data that is generated from $f(t)$

The two curves display good fit in the Laplace domain, establishing that the algorithm for the numerical Laplace Transformation of sample data is valid for our single compartment model. However, since our work focuses on the application of history matching, we would like to confirm that the model parameters obtained from the curve fitting exercise are unique and match the true/given parameters. Using the curve fitting tool available in Matlab, we match the numerical Laplace Transform of the data to the

model $\dfrac{A}{\sqrt{s}}\tanh\left(B\sqrt{s}\right)$, and the results of the parameters with 95% confidence level and

1.000 in coefficient of determination are as follows:

$$
\begin{aligned}
A &= 0.9982 \\
B &= 1.001
\end{aligned}
\qquad (3.9)
$$

The model parameters A and B match closely to the true parameters with the relative percentage error of 0.18% and 0.10%, respectively. Therefore, we can finally establish that the algorithm to transform discrete data in Laplace space and the uniqueness of the solutions to the single compartment model are appropriate for use in this study.

3.5.2 Test function #2

The second test function involves the solution to the dual compartment linear flow model derived in section 2.3 Thus, the test function #2 has the following form in the Laplace domain:

$$
G(s) = A\sqrt{\frac{B}{Cs} + \left(\frac{1}{Cs}\right)^{3/2} \sqrt{\frac{D(1-B)}{3}}\tanh\sqrt{\frac{3(1-B)Cs}{D}}\tanh\left(\sqrt{Bs + \sqrt{\frac{D(1-B)Cs}{3}}\tanh\sqrt{\frac{3(1-B)Cs}{D}}}\right)}
$$

(3.10)   where $A = 1.000e+04$, $B = 1.000e-03$, $C = 1.000e+02$, and $D = 1.000e-05$.

Since there is no analytical expression of $g(t)$, the inverted function of $G(s)$, one has to obtain $g(t)$ via numerical inversion methods, one such as the Gaver-Stehfest algorithm which is studied in detail in Appendix C. Figure 11 presents the log-log graph of $g(t)$ versus t.
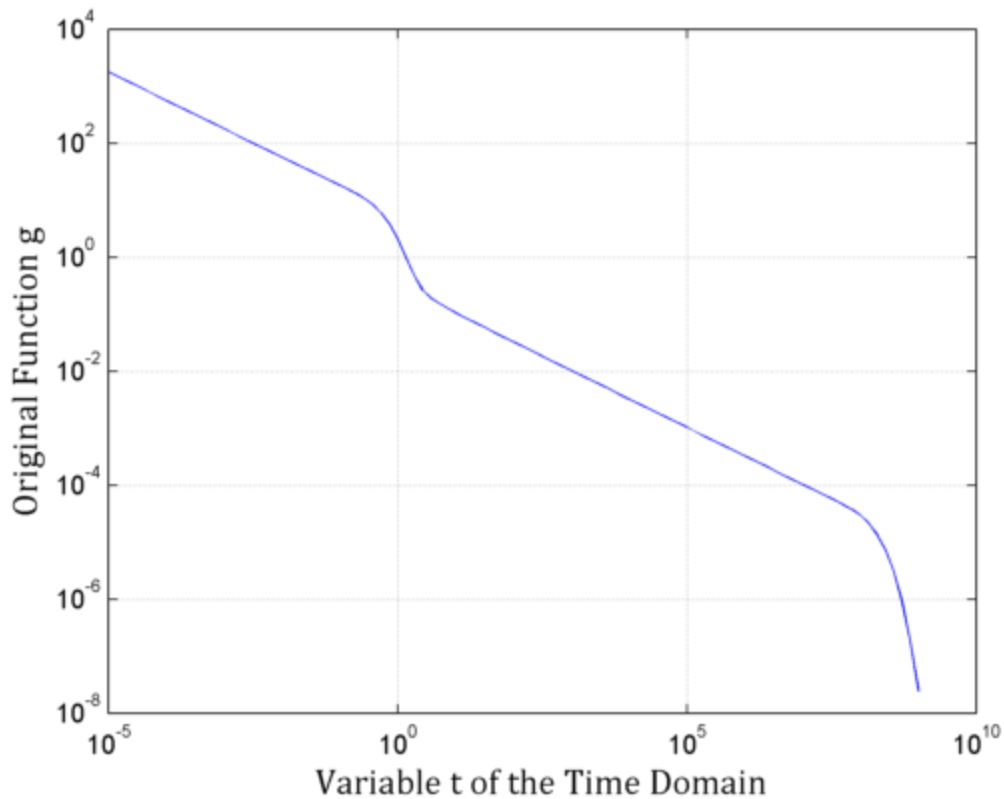
Figure 11:　Function $g(t)$ evaluated numerically through the Gaver-Stehfest's inversion of its Laplace Transform $G(s)$

Figure 11 displays the two-timescale that we expect to observe from a dual compartment linear flow. As the underlying physics depicts a complex real-time behavior, developing a best-fit line for the function $g(t)$ is not an easy task. However, in the Laplace domain, function $G(s)$ displays a more smoothing behavior that again confirms the superiority of our method of history matching in this alternative space. Figure 12 plots the function $G(s)$ and the numerical Laplace Transform of the data generated from the original function $g(t)$ are plotted against the variable s of the Laplace domain.
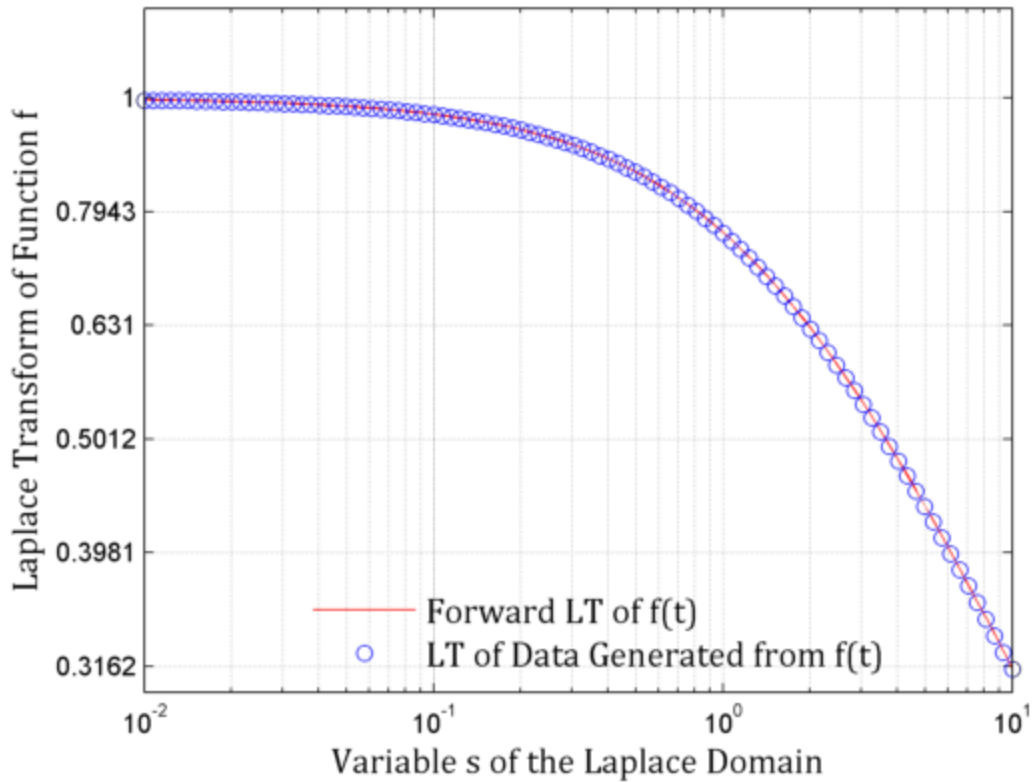
41
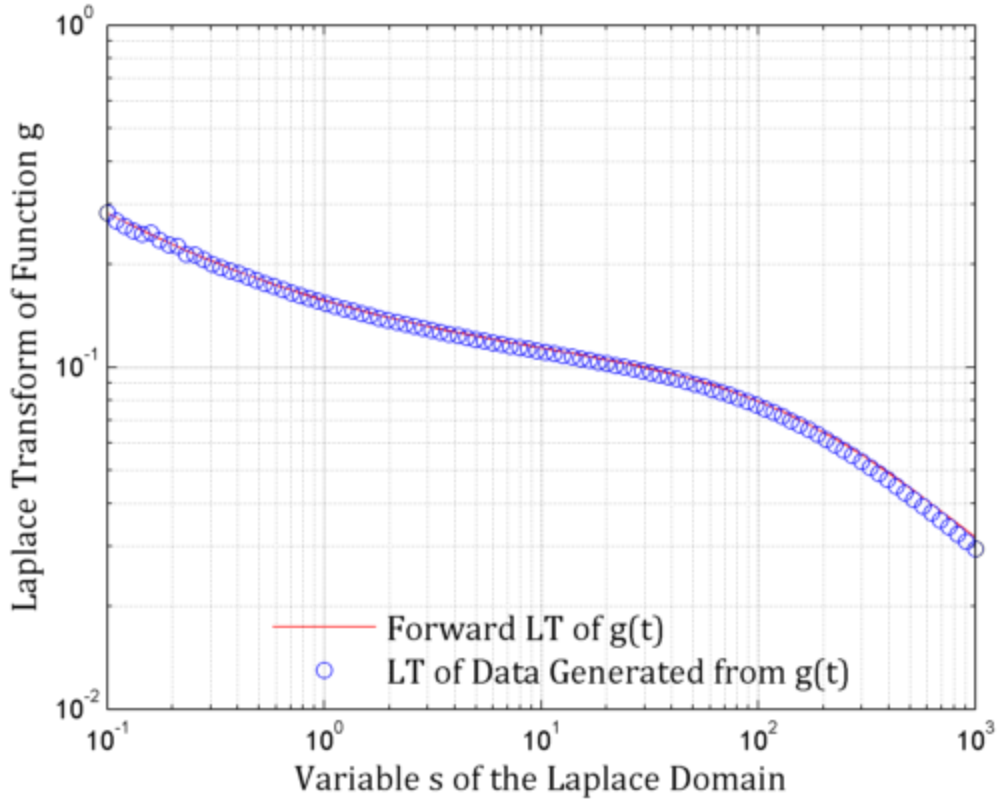
Figure 12: The comparison between $G(s)$ and the numerical Laplace transform of the
data that is generated from $g(t)$

The two curves display good fit in the Laplace domain, establishing that the algorithm for the numerical Laplace Transformation of sample data is valid for the dual compartment model. However, since our work focuses on the application of history matching, we would like to confirm that the model parameters obtained from the best-fit in the Laplace space are unique and match the given parameters. Using the curve fitting tool available in Matlab, we match the numerical Laplace Transform of the data to the

model: $A\sqrt{\dfrac{B}{Cs}+\left(\dfrac{1}{Cs}\right)^{3/2}}\sqrt{\dfrac{D(1-B)}{3}}\tanh\sqrt{\dfrac{3(1-B)Cs}{D}}\tanh\left(\sqrt{Bs+\sqrt{\dfrac{D(1-B)Cs}{3}}\tanh\sqrt{\dfrac{3(1-B)Cs}{D}}}\right).$

42

We find that there are no unique solutions to the problem. However, if we reduce the number of unknown variables down to three, then the solutions are unique. For instance, if we fix the value of A to be $1.000e+04$, then we obtain a unique fit with 95% confidence level and 0.9999 in coefficient of determination with the following parameters:

$$B = 9.946e-04$$
$$C = 1.039e+02 \qquad (3.11)$$
$$D = 9.994e-06$$

The variables B, C, and D match closely to the true parameters with the relative percentage error of 0.54%, 3.9% and 0.06%, respectively. Similarly, if the value of any one of the four original variables is fixed, we obtain the results of the other three parameters with similarly high values of R-squared and low value of relative error. Therefore, we can finally establish that both the algorithm to transform discrete data in the Laplace space and the dual compartment model (with one less unknown parameter) are appropriate for use in this study.

Chapter 4: Applications

4.1 A NEW METHOD OF HISTORY MATCHING

Whereas the previous chapters equip us with mathematical background and tools, the current chapter focuses on the interesting applications that this thesis lays the groundwork for- history matching in a domain different from the time domain to obtain useful reservoir parameters.

Since the novel history matching method happens in the Laplace space, one needs to first acquire a Laplace model, a function of s that contains unknown parameters. This step is simple enough since most differential equations governing the reservoir flow can be solved by the Laplace Transform method. In the conventional method, obtaining an analytical model often presents complication since the analytical solution in the time domain is not always available.

The data of reservoir engineering problems, specifically flow rate and pressure are recorded in real time, hence the second step involves transforming data into the Laplace domain. This comprises one of the most important steps. Since the data before the first data point and that after the last data point are often missing, it requires that we have an accurate knowledge of the functional representation of the early-time and late-time extrapolation. Otherwise, we could encounter troubles fitting the transformed data with the model. Since our variable of interest is now the Laplace variable s, we also need to determine the range of s of interest. As s is the inversion of time, as a rule of thumb, s is chosen to be in the range of $\left(\dfrac{1}{t_{max}}, \dfrac{1}{t_{min}} \right)$ but the situation may vary from case to case.

44

The third step is history matching the transformed data with the model in Laplace domain through which we can obtain the fitting parameters. These lumped parameters are functions of reservoir properties and well configurations. As the parameters are lumped together, prior knowledge of some of the individual parameters must be known in other to seek for other individual parameters. Most importantly, we can obtain an approximate to the estimated ultimate recovery from the lumped parameters, as discussed in the previous chapter.

The last step is to double check the results of the history matching. If we stop at the last step, readers may question if a best fit in the Laplace domain guarantees the same in the time domain. We assure you that it does by providing a plot that compares data and model in the time space- what readers often would like to see. Now, the model in the time domain can be obtained via analytical Laplace transformation or numerical methods, one such as the Gaver-Stehfest algorithm. The original data is then plotted in conjunction with the model in the time domain. If the history matching job is good enough, we could use the real-time model for forecasting. We will explore several examples in the coming sections.

4.2 INTRODUCTION TO THE DATA SET

The data used in this study comes from a liquid-rich shale play in North America. This data set contains data from 104 wells of varying completion properties. Geologic data such as initial reservoir pressure and reservoir depth are given. Oil production rates, water production rates, and tubing head pressures are recorded on a daily basis. A production period begins when the well starts producing or returns to production once

shut in, and ends when the well shuts in the next time. A well often undergoes more than one production periods. Four main observations and assumptions are made as follows:

(1) The amount of water produced from these wells is relatively low and constant, making the assumption of oil being the only flowing phase appropriate.

(2) According to Ogunyomi (2014), production data from most fractured-horizontal wells in gas and liquid-rich unconventional reservoirs plot as straight lines with a one half-slope on a log-log plot of rate versus time. This half-slope line characterizes the transient flow from the reservoir matrix to the fracture. Figure 11 shows a typical rate plot of a well chosen at random, and it bears similar production signature.

(3) A shut in period is often identified as a period of time in which the producing rates and the tubing head pressures remain consistently zero for more than two days. A well may experience more than one periodic shut-in.

(4) We can calculate the well flowing pressure from the tubing head pressure data assuming constant hydraulic gradient.

(5) Pressure is relatively constant except for when production starts or resumes after well shut-in.

4.3 SINGLE VERSUS DUAL COMPARTMENT MODELS- CONSTANT FLOWING PRESSURE

This section consists of two history matching exercises using two models: the single compartment and the dual compartment models on the same well (UT ID 79) both schemes assuming constant BHP. Two history match cases are shown in detail below:

46

4.3.1 Single Compartment Model

First of all, we would like to obtain a visual of the well's general production behavior. Figure 13 presents the distribution of the production rate and tubing-head pressures of that well over time. No gas is produced during the entire production period, indicating that the BHP is well above the bubble point pressure.
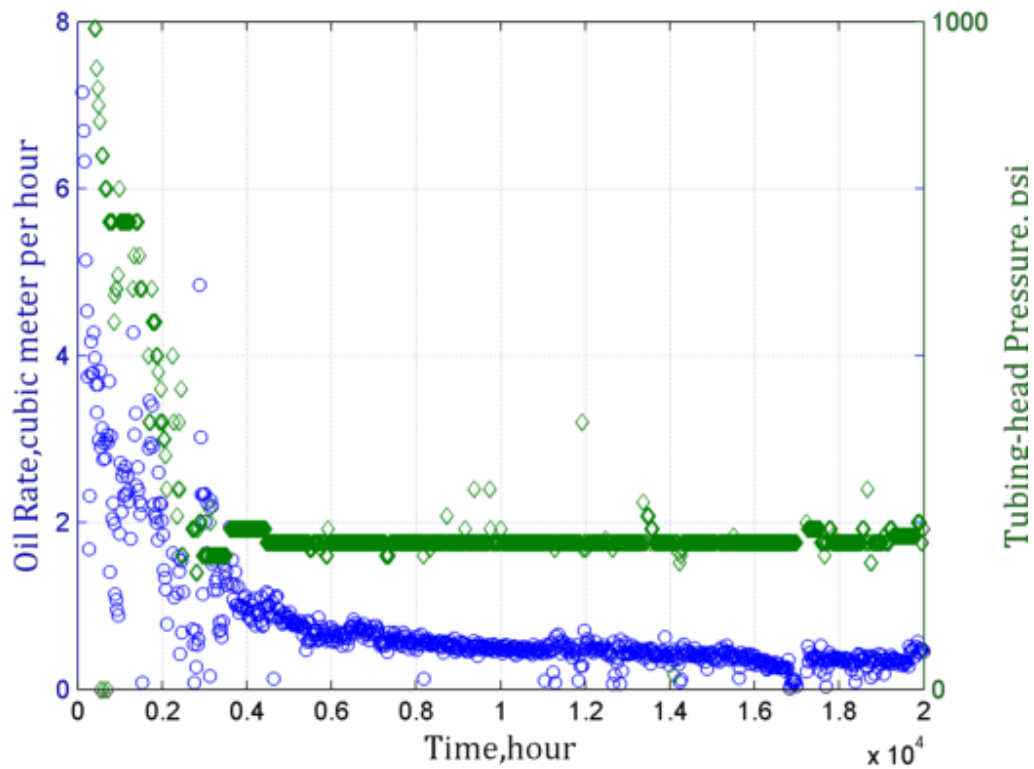
Figure 13:   Produced oil rate and tubing-head pressure of the well UT-ID 79

It appears that there is only one production period from beginning to end, and there is not a scheduled shut-in during the production course of the well. We observe that tubing-head pressure drops quickly in the beginning then stays relatively constant at

around 200 psi. The production rate data are transformed into the Laplace domain and fitted to the constant BHP Laplace model, as shown below in Figure 14.
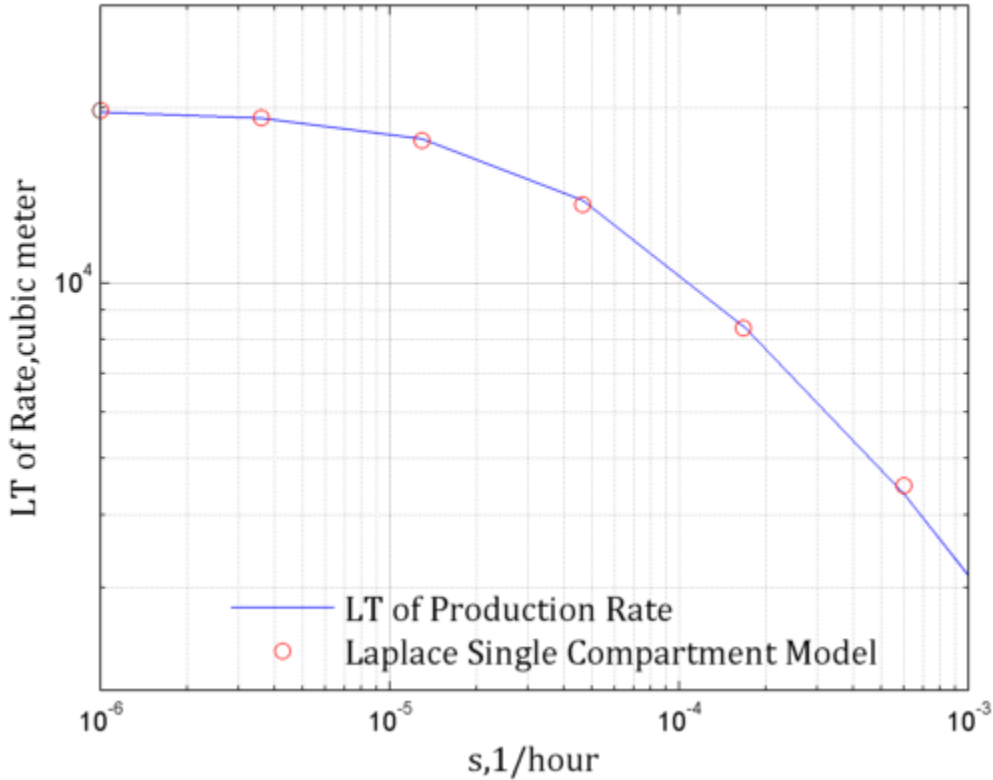
Figure 14:   Transformed oil rate data of well UT-ID 79 fitted to the constant BHP single compartment model in Laplace domain.

The transformed oil rate data in the Laplace space displays a smooth curve even though the original data in the time domain shows significant scatter. Therefore, the step of smoothing out the data to cancel noise is eliminated, and that is one of the advantages of this method. As mentioned earlier, fitting in the Laplace space with a Laplace model is superior to the traditional method as it gives a good, and unique fit. The coefficient of determination is at 0.9927. The model parameters obtained are as follows:

$$\begin{cases} E = 112.2 \dfrac{m^3}{\sqrt{hr}} \\ F = 175.1\sqrt{hr} \end{cases} \qquad (3.12)$$

With these model parameters, the best-fit is now complete. Next, we would like to verify the fit and turn it into something useful. We could justify the results by applying the estimated parameters to the analytical or numerical real-time model and comparing the computed results to the original data. An analytical inversion of the Laplace solution exists for the single compartment model. First, the volumetric oil rate is tested as Figure 6 plots the original produced oil rate together with the real-time model.
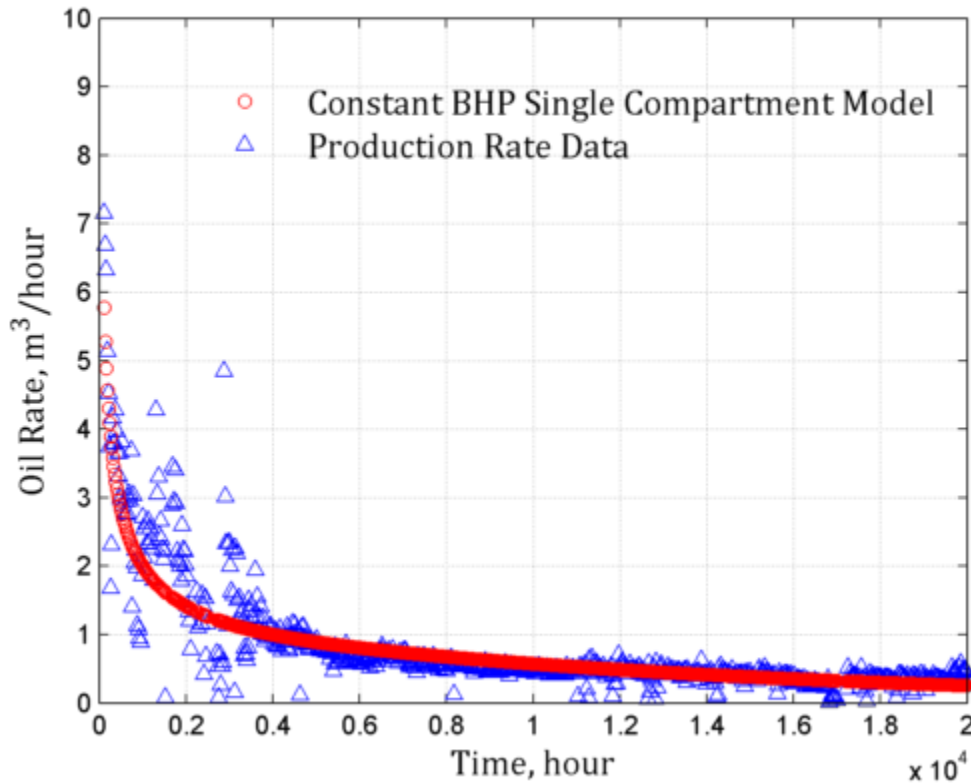
Figure 15:   Original production data of well UT-ID 79 compared to the constant BHP single compartment model for rate in the time domain

As shown in Figure 15, the constant BHP single compartment model fits the production rate nicely in the time domain. The large deviation of the data from the model at around 2000 to 3000 hours into production, can be explained due to the unstable well flowing pressure as observed in Figure 13, which violates the model assumption of constant pressure. If computed at a later time, the real-time model allows one to forecast the future production rate, thus becoming an excellent tool when making engineering or management decision.

A second way of validating the results is to apply the same estimated parameters to the equation of cumulative volume as derived in (2.20). Figure 16 plots the original cumulative produced oil data together with in comparison to the real-time model.
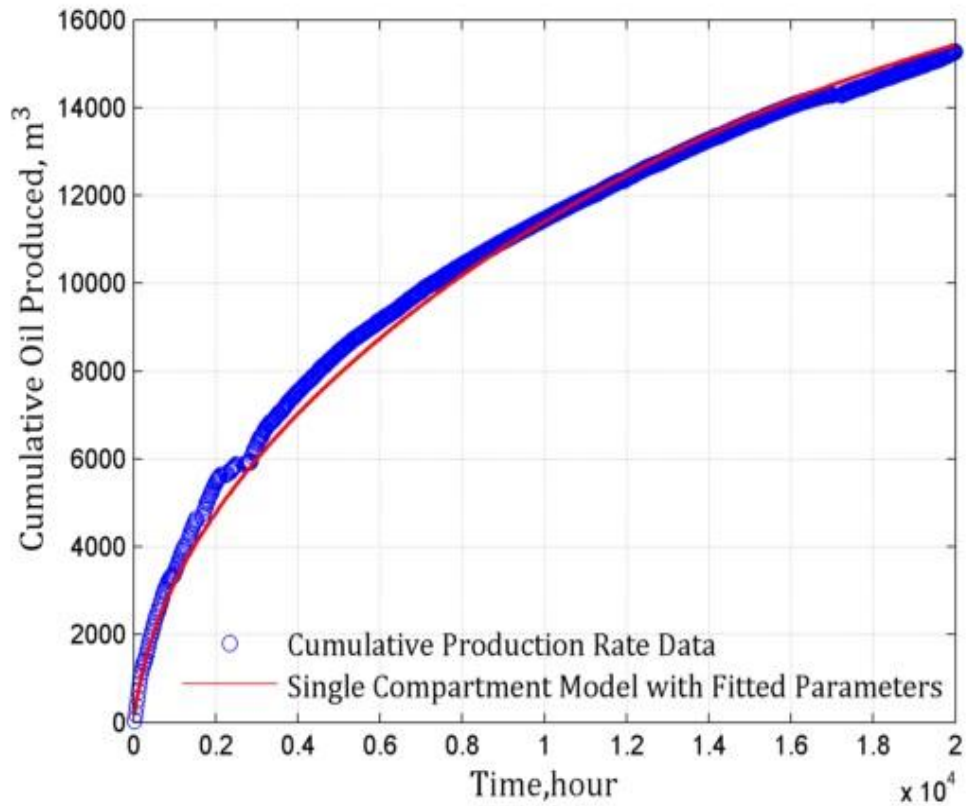
Figure 16:   Cumulative production data of well UT-ID 79 is compared to the results of the constant BHP single compartment model for cumulative volume in the time domain

As shown in Figure 16, the current model fits the cumulative production data nicely in the time domain. Provided that there is no major change in the production operations, we can determine the production life of the well by equating the expression of the cumulative volume as found in Equation (2.20) to the estimated total drainage volume calculated via the model parameters.

4.3.2 Dual Compartment Model

We now apply the dual compartment model to the previously studied data set from well UT ID 79. The production rate data are transformed into Laplace domain and fitted to the dual compartment model in Laplace.
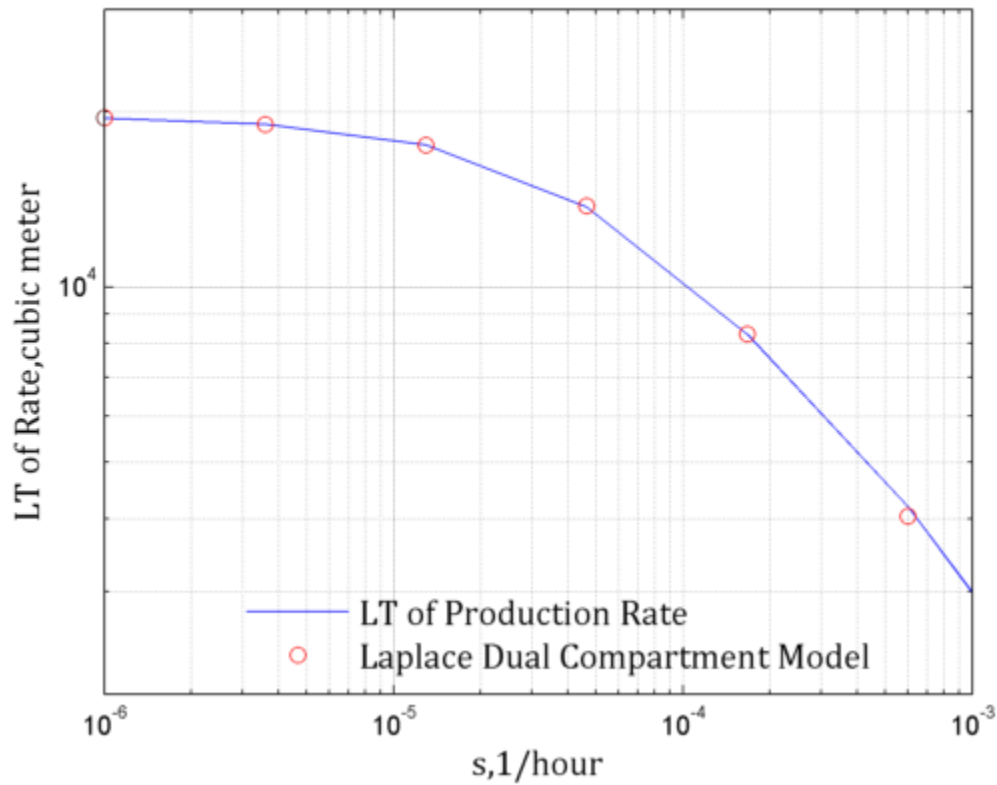
Figure 17: Transformed oil rate data of well UT-ID 79 fitted to the dual compartment model in Laplace domain

As shown in Figure 17, the dual compartment model gives a better fit compared to the single compartment to the production data in Laplace domain, i.e. the coefficient of determination is at 0.9996 which is slightly higher than the value 0.9927 in the single compartment case. The best-fit provides us the following four parameters:

$$\begin{cases} a = 1.965e + 04m^3 \\ c = 3.206e + 03hr \\ \omega = 5.109e - 04 \\ \lambda = 0.3741 \end{cases}$$

Interestingly, in this case, without even constraining the value of any of the four variables, we are able to obtain unique solutions, hence assuring the accuracy of the model parameters. Since the real-time solution for rate cannot be inverted analytically from Laplace rate solution, the Gaver-Stehfest algorithm is employed to obtain the numerical inversion of the Laplace rate. The production rate data is then compared to the numerical approximation of the model obtained via the Gaver-Stehfest method for $N = 14$, shown in Figure 18.
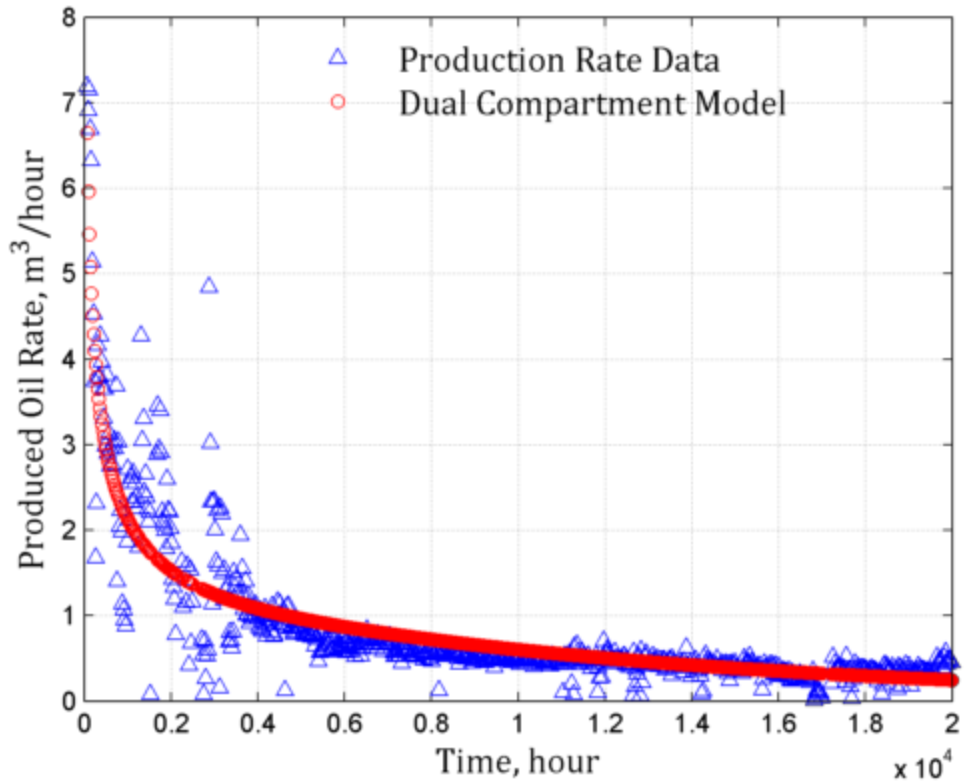
Figure 18:   Original production rate of well UT-ID 79 compared to results from the dual
              compartment model in the time domain.

As shown in Figure 18, the dual compartment model fits comparably well to the produced oil rate as the single compartment model, however comes with slightly higher computational cost than the latter.

Additionally, we may also validate the estimated parameters based on the cumulative oil volume. Again, the numerical approximation of the real-time cumulative volume can computed via the Gaver-Stehfest algorithm for $N = 14$. Figure 19 plots the original cumulative produced oil data in comparison to the model for cumulative volume as found in Equation (2.47).
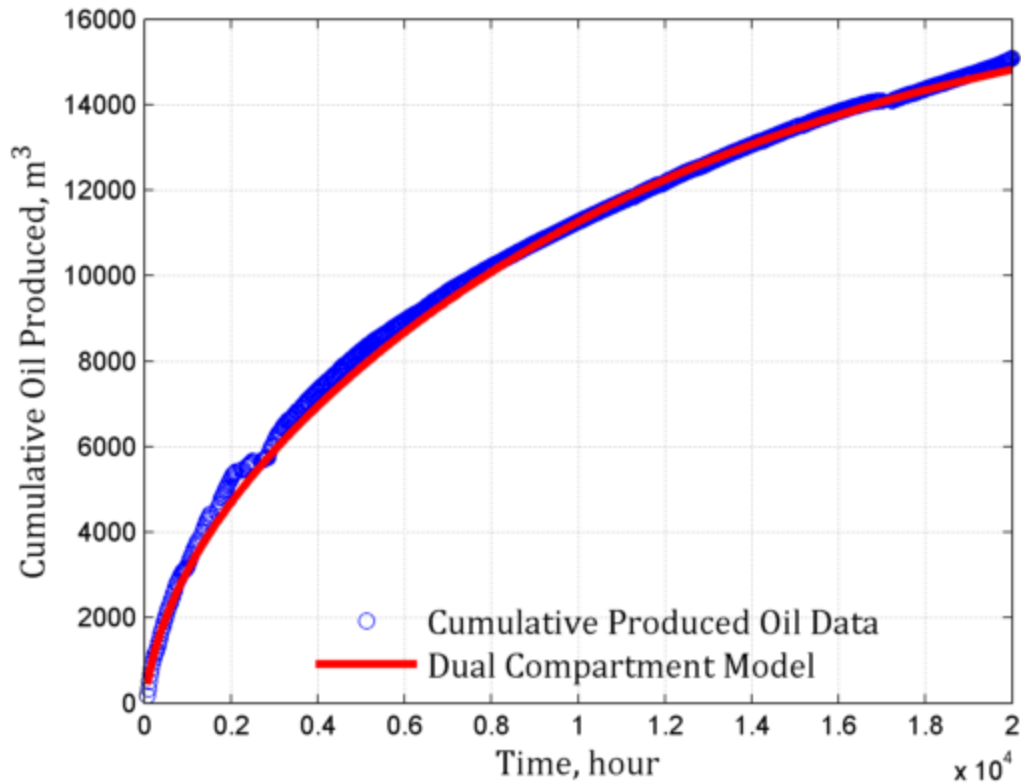
Figure 19:   Cumulative oil production data of well UT-ID 79 compared to the results of the dual compartment model in the time domain

As expected, the dual compartment model fits the cumulative produced oil data excellently. Since an analytical form of the solutions to this model does not exist in the time domain, finding the production life of the well is not as straightforward as with the single compartment model but is still possible with some numerical methods.

The objectives of section 4.3 are two fold. The first is to validate the effectiveness of the novel method of history matching. The two exercises above prove that this method is not only simple but also effective in history matching flow data in fractured tight formations. The advantages of this method over the traditional procedure of history

55

matching in the time domain is its ability to model the reservoir flow using different compatible physics models as well as multiple compartment models. And regardless of the models we use, the method proves to work well with exceptional accuracy. The second objective is to understand the relationship between the computational power, the accuracy and the number of unknown variables. Clearly, increasing the number of unknown parameters by increasing number of compartments in the model hinders the computational speed while matching however compensates for insignificant accuracy improvement. In depth analysis of the two models is further discussed in section 4.5

4.4 CONSTANT VERSUS VARIABLE WELL FLOWING PRESSURE SINGLE COMPARTMENT MODELS

Within this section, we perform history matching exercises using the single compartment model, as we just find that single compartment is adequate to handle our data set, with two different assumptions: constant, and variable BHP. With the traditional method, incorporating the variability of the BHP to the best fit of the produced oil rate data in the time domain is almost impossible since the model itself would entail numerical approximation of an integral involving the BHP. The novel history matching method in the Laplace domain allows one to extract meaningful reservoir parameters from the analytical closed-form solution in the Laplace space which includes simple expression of the Laplace transform of the BHP, as derived in Equation (2.26).

4.4.1 Constant BHP Single Compartment Model

In this section, we apply the constant BHP single compartment model to a different well in the data set, namely UT-ID 290. The plot of the production rate and the

tubing head pressure is shown in Figure 20 to help readers with understanding this particular well behavior.
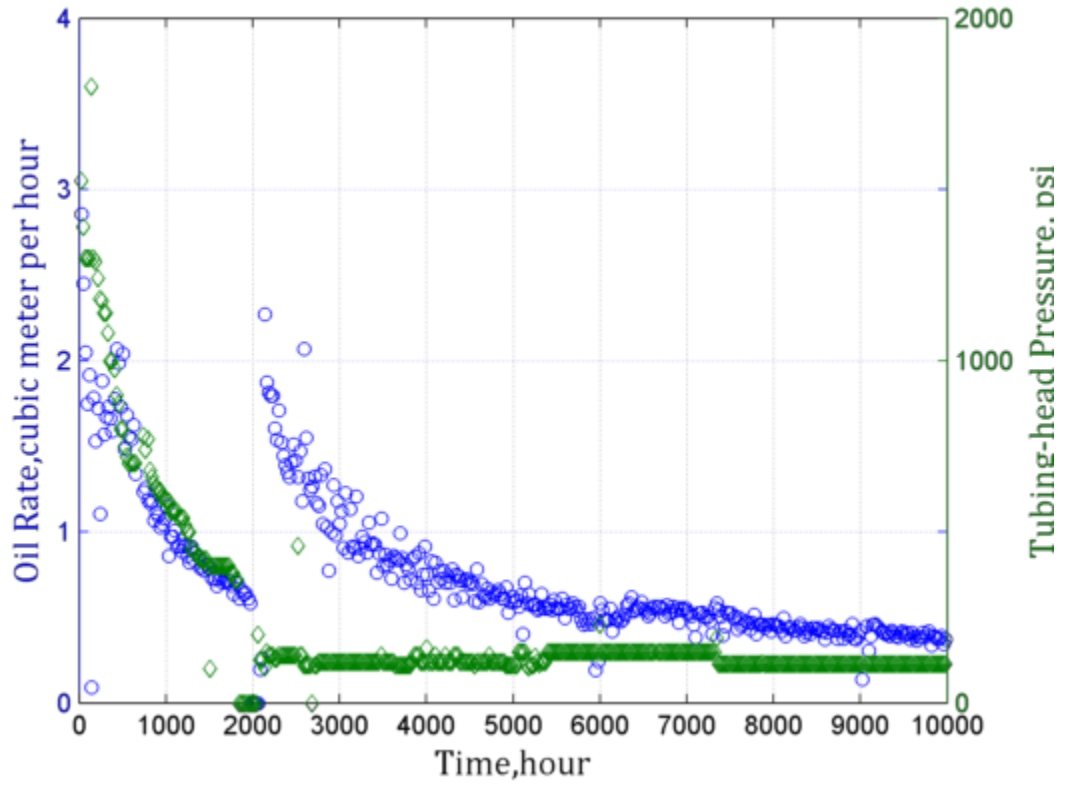
Figure 20:   Variation of oil rate and the tubing-head pressure of well UT-ID 290
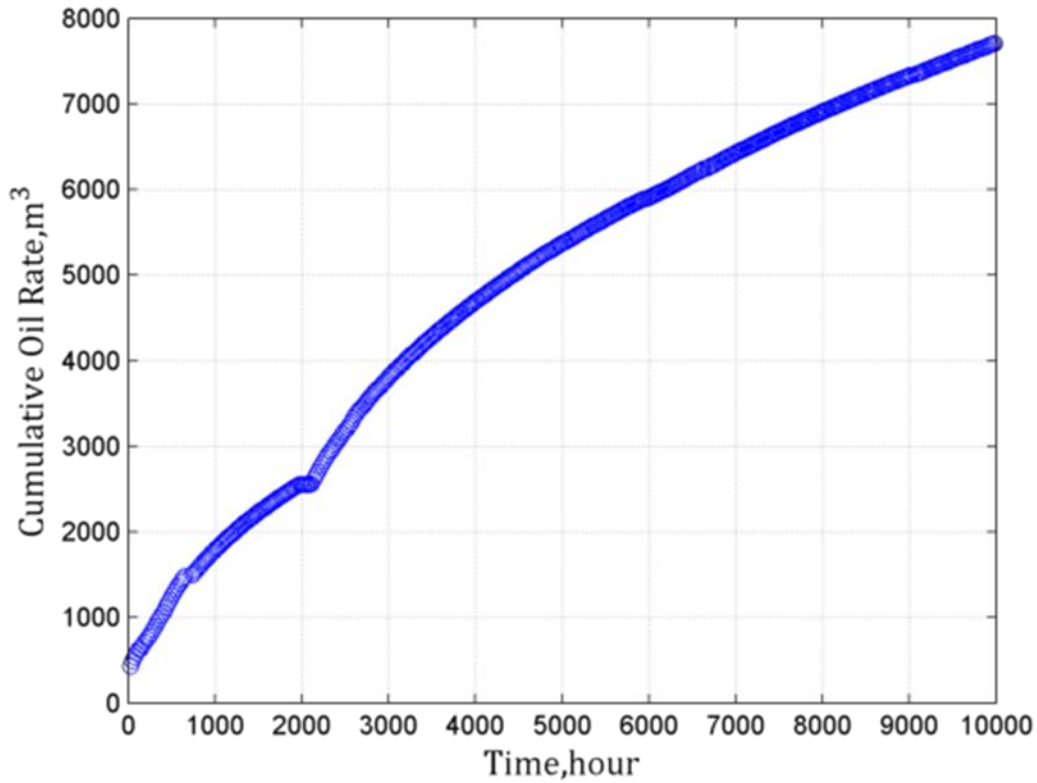
Figure 21:   Variation of the cumulative oil volume produced from well UT-ID 290

Figures 20 and 21 clearly display two production periods. In the initial period, oil is assumed to flow freely for approximately 2000 hours. The second peak takes place after about 2000 hours into production after a period of shut-in during which the well's tubing-head pressure and production rate remains zero for several days. During this time, reservoir pressure builds up until production resumes. This second production period observes relatively constant tubing head pressure because of operational control. In the Laplace domain, Equation (2.30a) is used once to model the transformed rate data, and to obtain the model reservoir parameters. However, to display the match in the time domain, different versions of Equation (2.30b) are used to model different production periods: we

must shift the time of the next production period back by the time corresponding to the point of shut-in.

In the first scenario, the transformed production rate data is fitted to the constant BHP single compartment model in the Laplace domain. The obtained model parameters are as follows:

$$\begin{cases} E = 52.9 \dfrac{m^3}{\sqrt{hr}} \\ F = 144.8\sqrt{hr} \end{cases}$$

Using analytical real-time model is presented in equation plus the principle of time superposition, the original production data is then fitted with the constant BHP single compartment model in the time domain, shown in Figure 22.
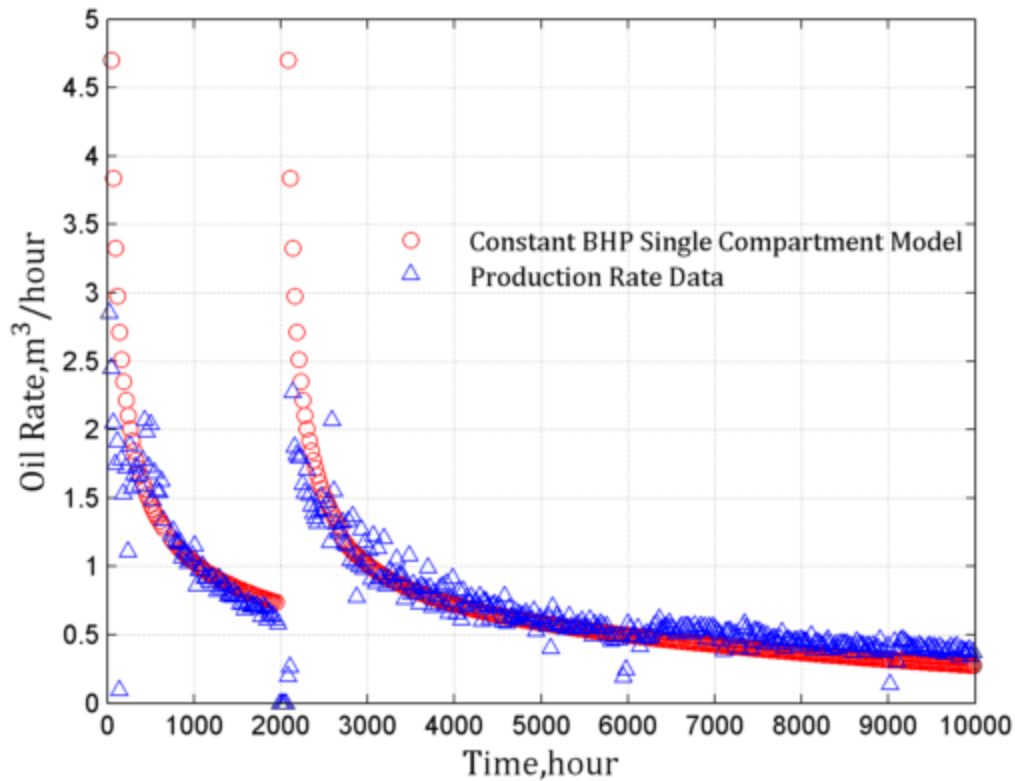
Figure 22:   Comparison of fits of original production data of well UT-ID 290 using the
constant BHP, single compartment model in the time domain.

Figure 22 shows a fairly good fit of the constant BHP single compartment model

to the production rate data. The model under-predicts the actual produced oil rate after

around 6000-7000 hours of production as a result of the adjustment (lowering) of the

tubing head pressure. Therefore, the model lacks the flexibility to handle fluctuations in

the well flowing pressure.

4.4.2 Variable BHP Single Compartment Model

In the second scenario, we apply the variable BHP single compartment model to

the same well (UT-ID 290). This model takes into the account the variable data of BHP

using the principle of time superposition. Assuming that there is a constant pressure difference between the tubing-head pressure and the BHP due to the pressure head of fluids in the wellbore, we can estimate the distribution of BHP over time. We also assume, though not necessarily accurate that during the shut-in period and right when production resumes, BHP equals the initial reservoir pressure.

In this scenario, both production data and estimated BHP data are transformed into the Laplace domain. The obtained model parameters are as follows:

$$\begin{cases} K &= 2.572\dfrac{m^3}{MPa\sqrt{hr}} \\ F &= 144.8\sqrt{hr} \end{cases}$$

Using analytical real-time model is presented in equation plus the principle of time superposition, the original production data is then fitted with the variable BHP single compartment model in the time domain, shown in Figure 23.
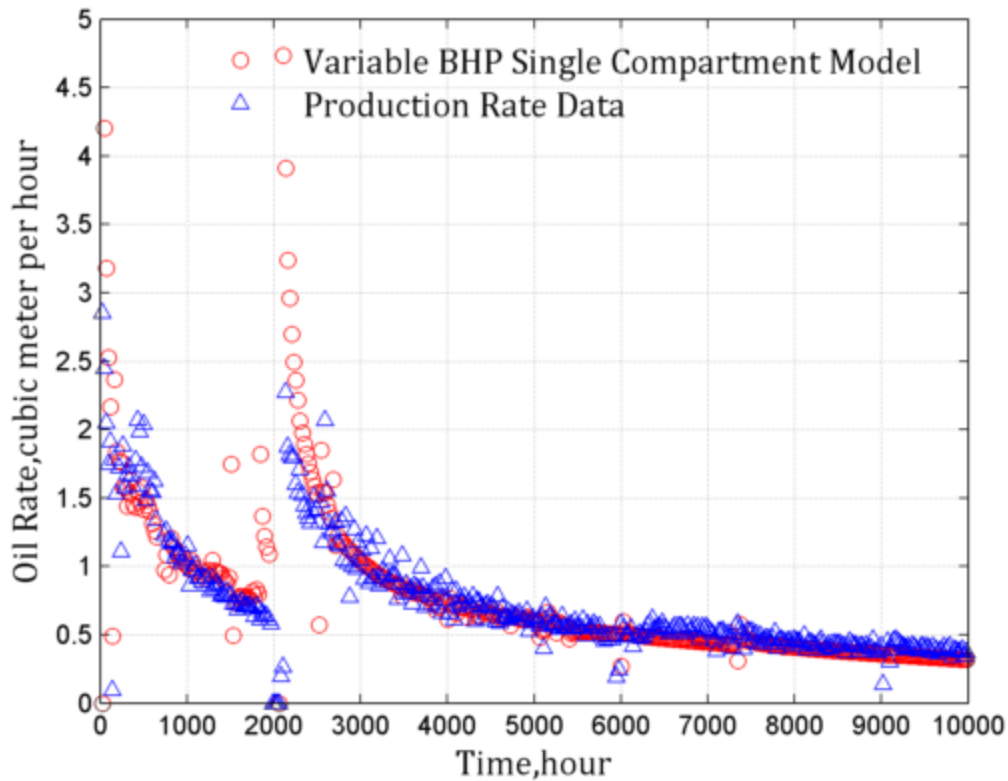
Figure 23:   Comparison between original production data of well UT-ID 290 and the fitted variable BHP, single compartment model in the time domain.

As shown in Figure 23, the variable BHP single compartment model gives a better fit to the production data than the constant BHP single compartment model, however comes with a much higher computational cost due to the complexity of the numerical approximation of convolution. The overestimation of the producing rate at the beginning of each production period is the result of unreliable estimation of the reservoir pressure: the pressure at time $t = 0$ and the reservoir pressure after the shut-in period are assumed to equal the initial pressure reported in the data.

4.5 ANALYSIS

4.5.1 Single versus Dual Compartment Models

Two models whose Laplace solutions are readily available are studied side-by-side for well UT-ID 79, a single compartment (flow from matrix to a stimulated reservoir volume) model versus a dual compartment (matrix to a stimulated reservoir volume to a wellbore) model. One of the immediate applications of fitting the production data to the models is to determine the reservoir parameters. Since both models stand on the same physic, the ultimate recovery estimated using either the single or the dual compartment models should be consistent. The drainage volume can be computed from the single compartment model parameters, as derived in equation. This value can be calculated as $EUR_{single} = E.F = 19,646 m^3$. In the dual compartment model, the drainage volume is conveniently one of the model parameters, a, as shown in equation 2.2.4; therefore $EUR_{double} = 19,650 m^3$. The drainage volume estimated from both models are similar, proving their robustness.

Other than the drainage volume, the two models deliver results of different reservoir parameters due to the different assumptions: the single focuses on the matrix (as the volume of the fracture is insignificant), while the dual provides knowledge on the combination of fracture and matrix properties. To ensure solutions uniqueness, as discussed in (), the single compartment model is recommended to obtain the matrix properties, and then to calculate the estimated ultimate recovery. The dual compartment model, if constrained by the drainage volume estimated from the single model, would

provide better accuracy and uniqueness to the fracture/matrix reservoir parameters. Ultimately, what we want to achieve is estimating the ultimate recovery; hence the single compartment model is good enough to perform the task with given its simplicity and computational efficiency.

Theoretically, the early production rate from the fractured wells should display a one half-slope line on a log-log plot, which corresponds to the early fracture transient flow; however, this period is too short to be discernable, and is often unaccounted for in a daily recorded data. Following this fracture-flow period, production rate displays another straight line with a one half-slope on a log-log plot, which refers the predominant matrix transient flow. The reservoir matrix boundary is reached at the end of the transient flow after which production rates decline exponentially. The single compartment model is designed to characterize matrix transient flow then boundary-dominated flow regimes which sometimes last almost as long as the economic life of the well, hence is adequate to analyze flow performance in these wells.

The variables k_m and d represent the characteristic microscopic and macroscopic length scale of the matrix, respectively. If we define the matrix time constant as $\tau_m = d^2/\alpha_m$ where $\alpha_m = k_m/(\phi \mu c_t)_m$, then τ_m characterizes flow in the matrix and indicates how quickly the parallel fractures communicate to each other. This value can be obtained through the single compartment model parameters: $\tau_m = F^2$. In fractured tight reservoir, we expect a high value of the matrix time constant because of the ultra-low matrix permeability in the denominator. For well UT-ID 79, the matrix time constant is

64

calculated to be: $\tau_m = 30,660 \, hr$. Similarly, k_f and x_f represent the characteristic microscopic and macroscopic length scale of the fracture, respectively. If we define the fracture time constant as $\tau_f = x_f^2 / \alpha_f$ where $\alpha_f = k_f / (\phi \mu c_t)_f$, then τ_f characterizes fracture flow and indicates how quickly the tips of each transverse fracture communicate to each other. This value can be computed through the dual compartment model parameters: $\tau_f = c.\omega$ and in this particular example, $\tau_f = 1.6 \, hr$ which is five orders smaller than τ_m. Justifiably, since the fracture permeability is much larger than the reservoir matrix permeability, it takes much shorter time for the fracture tips to interact.

4.5.2 Constant versus Variable Well Flowing Pressure Single Compartment Models

Two scenarios of the single compartment model with different assumptions on the BHP, one with constant BHP and the other with variable BHP, whose Laplace solutions are readily available are studied side-by-side for well UT-ID 290. We find that the matrix time constant τ_m, a derivate of the parameter F, is constant in both scenarios and equals $20,967 \, hr$, indicating the robustness of the model.

The variable BHP single compartment is a more accurate model since it incorporates the real-time change of the tubing head pressure, enabling it to predict precise drawdown pressure. However, the variable BHP model comes with a computational cost due to the complexity of the convolution's numerical approximation. Furthermore, finding the estimated ultimate recovery with the constant BHP model is straightforward: $EUR = E.F = 7,660 \, m^3$. It is a little bit trickier for the variable BHP

model since $EUR = K.F\left(P_i - P_{wf}\big|_{t\to\infty}\right)$ where the initial pressure P_i is given to be

$7{,}088\,psi$, and $P_{wf}\big|_{t\to\infty}$ is approximated by the last value of the bottom hole pressure ,

which is recorded at $3{,}810\,psi$. Hence, the estimated ultimate recovery is computed to be

$8{,}421m^3$. Based on the plot of the cumulative volume of oil produced shown in figure

(), the last value of cumulative produced oil is $7{,}803\,m^3$, which exceeds the estimated

drainage volume from the constant BHP model. Again, the variable BHP model proves to

be more reliable in terms of providing accurate reservoir characteristics.

Chapter 5: Conclusions and Future Work

This chapter summarizes the conclusions of this thesis and presents recommendations for future works. This thesis focuses on deriving simple models that describe flow in fractured shale oil reservoirs. Previous attempts of using the empirical models that are developed based on the decline curve equation presented by Arps occasionally do not yield realistic estimated ultimate recovery and physical model parameters (Ogunyomi, 2014b). Thus we would like to develop analytical models based on the solutions to material balances.

Two analytical models are proposed: the single compartment and the dual compartment. The main difference between the two models is that the pore volume of the fractures in the single compartment model is assumed insignificant and pressure drop in fracture flow is neglected. Next, the models are employed for the purposes of history matching, reservoir characterization and production forecast. The typical approach to this reservoir engineering problem often requires one to arrive at a real-time, closed-form solution of the models; however, because of the complicated physics of most flow problems, that task becomes quite challenging.

Laplace transformation is one of the powerful methods to solve the differential equations of the flow problems because of its simplicity and flexibility to couple with almost all of the boundary conditions that exist in petroleum engineering. However the analytical inversion of the solutions from Laplace space to real time is complicated and often times unavailable, i.e., the dual compartment model. An alternative is to numerical

invert the Laplace solutions, however such numerical solutions have no insight in constructing meaningful models.

The novelty of this thesis involves proving that history matching of data to flow models in the Laplace space is beneficial, especially for tight fractured formations, as shown in our investigation. Two main results are observed:

(1) Both models objectively characterize the behavior of the theoretical data (from numerical simulation) as well as the field data (from the liquid-rich shale play in North America) while yielding realistic values of the expected ultimate recovery. The dual compartment model aims at depicting two timescales; one identifies early fracture flow, the other features matrix flow. However in reality, it is difficult to capture the full behavior with the field data; even if it exists, the fracture flow is too short-lived and the data is too scattered to be distinguishable while fitting. Fortunately, the single compartment model is proven to be effective for most field applications as its performance is as good as the dual compartment model.

(2) Since the solutions to differential equations are presented in the Laplace space, modeling of complicated flow problems become feasible, for instance, modeling multi-compartmental flow, and variable reservoir conditions etc. Particularly in this work, we had shown that fitting data to the dual compartment model is possible without a real-time analytical inversion. Additionally, we are able to model variable bottom hole

pressure without introducing inaccuracies introduced by numerical integration of convolution.

(3) Comparison with the models in the Laplace space requires an algorithm to transform data from the time domain to the Laplace domain. In this work, the method proposed by Onur and Reynolds (1988) proves to be accurate and effective in handling the transformation of discrete data. The algebraic curve-fitting procedure in the Laplace domain is shown in detail in this thesis. The smoothing nature of the Laplace transform enables one to eliminate data noise, reduce the computing time while objectively guaranteeing a best-fit.

This thesis work proves the effectiveness of handling data and obtaining useful parameters from data fitting in the Laplace space for engineering applications. The development of a reservoir simulation using a finite difference method that relies on discretizing the Laplace solution to the material balance equation on a grid is a frontier for the next generation of engineers. The new reservoir simulation tool eliminates the time dependency of the pressure equation, and thus the time discretization. As a result, timestep size does not compromise stability and accuracy unlike with the conventional reservoir simulation.

Appendices

This section of the thesis reviews some of the interesting properties of the Laplace Transform that readers might find useful to understand the derivations in this thesis.

A.1 Laplace Transform of a Time Derivative

Laplace transformation can be applied for any order of time derivative; however for the scope of this study, we are only interested in the first-order derivative. Let $f(t)$ and its first derivative $f'(t)$ be continuous for all real positive values of t, and of exponential order then:

$$\mathcal{L}\{f'(t)\} = s\mathcal{L}\{f(t)\} - f(0) = s\hat{f}(s) - f(0) \quad (A.1)$$

To prove this, we start with the definition of Laplace transform then perform integration by parts:

$$\mathcal{L}\{f'(t)\} = \int_0^\infty f'(t)e^{-st}$$

$$\int_0^\infty u\,dv = u\,v\Big|_0^\infty - \int_0^\infty v\,du$$

$$du = -se^{-st}dt \quad u = se^{-st}$$

$$v = f(t) \qquad dv = f'(t)dt \qquad\qquad\qquad (A.2)$$

$$\int_0^\infty f'(t)e^{-st} = [e^{-st}f(t)]_0^\infty - \int_0^\infty -f(t)se^{-st}dt$$

$$= [\underbrace{e^{-st}f(\infty)}_{0} - \underbrace{e^{-st}}_{1}f(0)] + s\int_0^\infty f(t)e^{-st}dt$$

$$= s\hat{f}(s) - f(0)$$

A.2 Laplace Transform of an Integral

Let $f(t)$ be a piecewise continuous function of exponential order s_0 on any finite interval in the range of real non-negative values of t. If $f'(t)$ is at least piecewise continuous on all real positive values of t then:

$$\mathcal{L}\left\{\int_0^t f(\tau)d\tau\right\} = \frac{\hat{f}(s)}{s} \quad \text{for } s > s_0 \qquad \text{(A.3)}$$

We prove it by using integration by parts again:

$$\mathcal{L}\left\{\int_0^t f(\tau)d\tau\right\} = \int_0^\infty (\int_0^t f(\tau)d\tau) e^{-st} dt$$

$$\int_0^\infty udv = u\,v\Big|_0^\infty - \int_0^\infty vdu$$

$$du = f(t)dt \quad u = \int_0^t f(\tau)d\tau$$

$$v = \frac{1}{s}e^{-st} \qquad dv = e^{-st}dt$$

$$\int_0^\infty (\int_0^t f(\tau)d\tau) e^{-st} dt = \left[-\frac{1}{s}e^{-st}\int_0^t f(\tau)d\tau\right]_0^\infty - \int_0^\infty (-\frac{1}{s}e^{-st})f(t)dt$$

$$= -\frac{1}{s}\left[e^{-st}\int_0^t f(\tau)d\tau\right]_0^\infty + \frac{1}{s}\int_0^\infty (e^{-st})f(t)dt$$

$$= -\frac{1}{s}\left[e^{-st}\int_0^t f(\tau)d\tau\right]_0^\infty + \frac{1}{s}\hat{f}(s)$$

$$= -\frac{1}{s}\left[e^{-st}\underbrace{\int_0^\infty f(\tau)d\tau - e^{-s0}\int_0^0 f(\tau)d\tau}_0\right]_0^\infty + \frac{1}{s}\hat{f}(s) \qquad \text{(A.4)}$$

The first term in the racket in the last equation goes to zero as the exponential term goes to zero faster than $f(\tau)$.

A.3 Superposition and Convolution

The principle of superposition is one of the most powerful tools in writing solutions to complex reservoir fluid flow problems without explicitly solving the differential equation involved. Mathematically, superposition states that any sum of individual solutions of a linear differential equation of any order is also a solution of the equation (Mian, 1992).

The diffusivity equation, a second-order differential equation, has been widely used in petroleum engineering to describe the fluid flow in porous media. The principle of superposition is valid since the diffusivity equation can be linearized because of the assumptions of small, constant fluid compressibility and small pressure gradient. Particularly, during a drawdown test, a well will be produced at different steady rates in different periods. The resulting pressure response of the well is the sum of the response from that well due to the original rate throughout the test and the responses from the superposed wells producing at the differential rates with respect to the original rate, from the time of rate switch until the end of the test (Satter, 2007). Mathematically speaking, superposition involves the operations of sum.

In this section, we will use the concept of superposition to understand convolution. Convolution can be regarded as the integral form of superposition. Let $f(t)$ and $g(t)$ be continuous or piece-wise continuous function of t, then the convolution integral of $f(t)$ and $g(t)$ is also a function of t and is defined by the following relation:

$$\psi(t) = f(t) * g(t) = \int_0^t f(t-\tau)g(\tau)d\tau \quad \text{(A.5)}$$

where $*$ is the convolution product, $\psi(t)$ is the convolution of $f(t)$ and $f(t)$, $g(t)$ is the unit impulse response or the influence function, and $f(t)$ is the forcing function. For the purpose of reservoir engineering, for instance, $f(t)$ is the known input of production rate, $g(t)$ is the reservoir model, then the desired output $\psi(t)$ is the pressure response. In that sense, convolution replaces the summation in superposition by an integral (Kuchuk 2010).

In Laplace domain, the integral convolution becomes a multiplication:

$$\mathcal{L}\{\psi(t)\} = \mathcal{L}\{f(t)*g(t)\} = \hat{f}(s)\hat{g}(s) \quad (A.6)$$

where $\hat{f}(s)$ and $\hat{g}(s)$ are the Laplace Transform of $f(t)$ and $g(t)$ respectively. It is often much easier to perform the convolution in the Laplace domain than when inverting back to the time domain. The application of the Laplace of the convolution integral will be examined closely in Chapter 3 of this thesis.

A.4 Dimensional Analysis

Laplace Transformation is the mapping of a function from the time domain to the frequency domain. For the exponential function e^{-ts} to exist, ts must be dimensionless; therefore s carries the unit of the inverse of time. Since the Laplace Transform of the function $f(t)$ involves the integration of $f(t)$ itself with respect to time, the Laplace Transform of the function $f(t)$ has the dimension of $f(t)$ multiplied by time. The derivative of function $f(t)$ has the dimension of $f(t)$ divided by time, thus the Laplace Transform of $f'(t)$ should have the dimension of $f(t)$. Similarly, the integral of $f(t)$ has

the dimension of $f(t)$ multiplying by time, hence the Laplace Transform of the integral $\int f(t)dt$ should have the dimension of $f(t)$ multiplying by the square of time. In conclusion, since the Laplace transform involves integration of an input function with respect to time, the unit of the resulting transform is that of the input function multiplying by time.

A.5 Limits of the Laplace Transform Inversion

Our works strongly involve the Laplace Transform, and it becomes increasingly important to study its limit. As it turns out, the theorems involving the long-time limit of the Laplace Transform become powerful tools in determining the original oil in place. The early-time and late-time behaviors are studied below:

A.5.1 Early-Time Behavior of the Laplace Transform Inversion

Let $f(t)$ be a function of t then the early-time behavior of $f(t)$ can be determined through its Laplace Transform's limit as s approaches infinity (Archer, 2000):

$$\lim_{t \to 0} f(t) = \lim_{s \to \infty} s\mathcal{L}\{f(t)\} \qquad \text{(A.7)}$$

A.5.2 Late-Time Behavior of Laplace Transform Inversion

This is also known as the Final Value Theorem in mathematical analysis. Let $f(t)$ be a function of t then the late-time behavior of $f(t)$ can be determined through its Laplace Transform's limit as s approaches zero (Archer):

$$\lim_{t \to \infty} f(t) = \lim_{s \to 0} s\mathcal{L}\{f(t)\} \qquad \text{(A.8)}$$

We should always check for unit consistency. The right side of the equation involves the product of s, of unit of time^{-1}, and $\mathcal{L}\{f(t)\}$, of unit of $f(t)$-time. This is consistent with the units of the left side.

In this thesis, we are not only concerned with modelling linear flow of fluid in hydraulically fractured, tight formation reservoirs, but we also attempt to model radial flow into the wellbore. The analytical solution to the radial diffusivity equation involves Bessel functions. We can find many approximate solutions to this problem in the literature, each often for a certain flow regime. We want to construct a simple solution that models not only infinite acting flow, but also boundary-dominated flow around the wellbore. First of all, it is important to study the limits of the Bessel functions before delving into the derivation of the model in Appendix C.

The upper limits of the modified Bessel functions of the first kind of order zero and one are given by:

$$\lim_{x \to \infty} I_0(x) = \lim_{x \to \infty} I_1(x) = \frac{e^x}{\sqrt{2\pi x}} \quad \text{(B.1)}$$

The upper limits of the modified Bessel functions of the second kind of order zero and one are given by:

$$\lim_{x \to \infty} K_0(x) = \lim_{x \to \infty} K_1(x) = \sqrt{\frac{\pi}{2x}} e^{-x} \quad \text{(B.2)}$$

The lower limits of the modified Bessel functions of the first kind of order zero and one are given by:

$$\lim_{x \to 0} I_0(x) = 1$$
$$\lim_{x \to 0} I_1(x) = \frac{x}{2} \quad \text{(B.3)}$$

76

The lower limits of the modified Bessel functions of the second kind of order zero and one are given by:

$$\lim_{x \to 0} K_0(x) = \frac{1}{2} \ln\left(\frac{4}{x^2}\right) - \gamma$$

$$\lim_{x \to 0} K_1(x) = \frac{1}{x}$$

(B.4)

APPENDIX C: THE GAVER-STEHFEST ALGORITHM FOR NUMERICAL INVERSION OF THE LAPLACE TRANSFORM

Laplace transformation is a useful tool that helps us solve any differential equation by transforming the equation and its initial or boundary values from the time domain into the Laplace domain. After solving the problem in the Laplace domain, we seek the inverse of the Laplace solution, thus solving the original initial value problem. The inverse Laplace Transform, also known as the real-time solution, can be found through analytical integration for the simple cases.

However, solving the differential equations that model fluid flow in porous media can be cumbersome, and arriving at a closed-form expression of the solutions can be rather challenging. Therefore, many researchers chose to direct their focus on numerical methods for solving more complex problems. There are several numerical algorithms for the inversion of the Laplace Transform in literature, and each method has its own applications and suitable types of functions. In the context of reservoir engineering, models are often only known in the Laplace domain for s, the Laplace argument, being a real number (Josso and Larsen, 2012). Therefore, the main criteria in selecting a numerical inversion algorithm are the inability to express models in the complex plane, and the stability as well as the accuracy. The Gaver-Stehfest method, which was developed in the late 1960's satisfies these criteria, therefore is one of the most widely used in reservoir engineering (Josso and Larsen, 2012). For these same reasons, we are going to employ the Gaver-Stehfest algorithm in this thesis.

C.1 The Gaver-Stehfest Algorithm

As mentioned earlier, for the Laplace solutions of most engineering problems to be useful in mathematical analysis, they must be inverted to the real-time domain via analytical inversion or numerical methods. The analytical inversion of most solutions is impossible due to their mathematical complexity. The Gaver-Stehfest algorithm provides a formula to numerically invert the Laplace Transform (Stehfest 1970). Assume that $f(t):(0,\infty)\mapsto R$ is a locally integrable function such that its Laplace Transform $F(s) = \int_0^\infty e^{-st} f(t)dt$ is finite for all $s>0$ and that $f(t)$ has no discontinuities or rapid oscillations, then $f(t)$ can be approximated by a sequence of functions of its forward Laplace Transform using the formula (Kuznetsov 2013):

$$f(t) = \left[s\sum_{n=1}^{N} K_n^N F(ns) \right]_{s=\frac{\ln 2}{t}} \qquad (C.1)$$

where the Laplace variable s is related to time t by the relation $s = \dfrac{\ln 2}{t}$. The weighting coefficients are given by the following formulas

$$K_n^N = (-1)^{n+\frac{N}{2}} \sum_{k=\frac{n+1}{2}}^{\min\left(n,\frac{N}{2}\right)} \frac{k^{\frac{N}{2}}(2k)!}{\left(\dfrac{N}{2}-k\right)!k!(k-1)!(n-k)!(2k-n)!} \qquad (C.2)$$

where N, the number of expansion terms, is an even integer (Chang 1989). The accuracy of the numerical inversion can be improved by increasing the value of N. However, the number of significant figures that the computational machine is able to hold

sets the upper limit of N for maximum accuracy (Moench et al. 1981). Moench and

Otaga was able to obtain accurate results by using $N = 18$ for double precision. Table 4

lists the coefficients for the Gaver-Stehfest algorithm up to $N = 18$. K_i^N denotes the

Gaver-Stehfest coefficient of the ith term in the N terms- expansion $(i \leq N)$

	K_i^2	K_i^4	K_i^6	K_i^8	K_i^{10}	K_i^{12}	K_i^{14}	K_i^{16}	K_i^{18}
K_1^N	2	-2	1	-3.333333E-01	8.333333E-02	-1.6666666E-02	2.77777777777E-03	-3.968253968253968E-04	4.960317460317460E-05
K_2^N	-2	26	-49	4.833333E+01	-3.208333E+01	1.6016666E+01	-6.40277777777E+00	2.133730158730159E+00	-6.095734126984128E-01
K_3^N	---	-48	366	-9.060000E+02	1.279000E+03	-1.2470000E+03	9.24050000000E+02	-5.510166666666667E+02	2.745940476190476E+02
K_4^N	---	24	-858	5.464666E+03	-1.562366E+04	2.7554333E+04	-3.45979277777E+04	3.350016111111111E+04	-2.630695674603174E+04
K_5^N	---	---	810	-1.437666E+04	8.424416E+04	-2.6328083E+05	5.40321111111E+05	-8.1266511111111111E+05	9.572572013888889E+05
K_6^N	---	---	-270	1.873000E+04	-2.369575E+05	1.3241387E+06	-4.39834636666E+06	1.007618376666667E+07	-1.735869484583333E+07
K_7^N	---	---	---	-1.194666E+04	3.759116E+05	-3.8917055E+06	2.10875917777E+07	-7.324138297777778E+07	1.824212226472222E+08
K_8^N	---	---	---	2.986666E+03	-3.400716E+05	7.0532863E+06	-6.39449130444E+07	3.390596320730159E+08	-1.218533288309127E+09
K_9^N	---	---	---	---	1.640625E+05	-8.0053365E+06	1.27597579550E+08	-1.052539536278571E+09	5.491680025283035E+09
K_{10}^N	---	---	---	---	-3.281250E+04	5.5528305E+06	-1.70137188083E+08	2.259013328583333E+09	-1.736213111520684E+10
K_{11}^N	---	---	---	---	---	-2.1555072E+06	1.50327467033E+08	-3.399701984433333E+09	3.945509690352738E+10
K_{12}^N	---	---	---	---	---	3.5925120E+05	-8.45921615000E+07	3.582450461700000E+09	-6.526651698517500E+10

K_{13}^N	---	---	---	---	---	---	2.74788847666E+07	-2.591494081366667E+09	7.873006832822083E+10
K_{14}^N	---	---	---	---	---	---	-3.92555496666E+06	1.227049828766667E+09	-6.855644419612083E+10
K_{15}^N	---	---	---	---	---	---	---	-3.427345554285714E+08	4.198434347505357E+10
K_{16}^N	---	---	---	---	---	---	---	4.284181942857143E+07	-1.716093471183929E+10
K_{17}^N	---	---	---	---	---	---	---	---	4.204550039102679E+09
K_{18}^N	---	---	---	---	---	---	---	---	-4.671722265669643E+08

Table 3: Coefficients for the Gaver-Stehfest algorithm

One of the advantages of the Gaver-Stehfest algorithm is that one is able to obtain a simple, closed-form approximate solution by using a small value of N. The extent of the accuracy of such solution depends on the smoothness of the function of interest. With table 4, users simply expand the sum of Equation (C.1) and plug in the appropriate coefficients.

C.2 Test Function

The purpose of this section is to check the validity of the Gaver-Stehfest algorithm and to decide the value of N to use for maximum accuracy of the numerical inversion, at least for the computer in use. The test function involves the dimensionless solution to the constant BHP single compartment linear flow model derived in section 2.1. Thus, it has the following forms in the Laplace and the time domains, respectively:

$$F(s) = \frac{1}{\sqrt{s}} \tanh\left(\sqrt{s}\right)$$

$$f(t) = 2\sum_{n=1}^{\infty} e^{\frac{-\pi^2 (2n-1)^2 t}{4}} \quad \text{(C.3)}$$

Function $f(t)$ is continuous and non-oscillatory on the interval $(0, \infty)$, hence satisfying the Gaver-Stehfest's functional requirement. Figure 24 depicts the comparison between the original function $f(t)$ and the numerical inversion of the Laplace transform $F(s)$ calculated for various values of N.
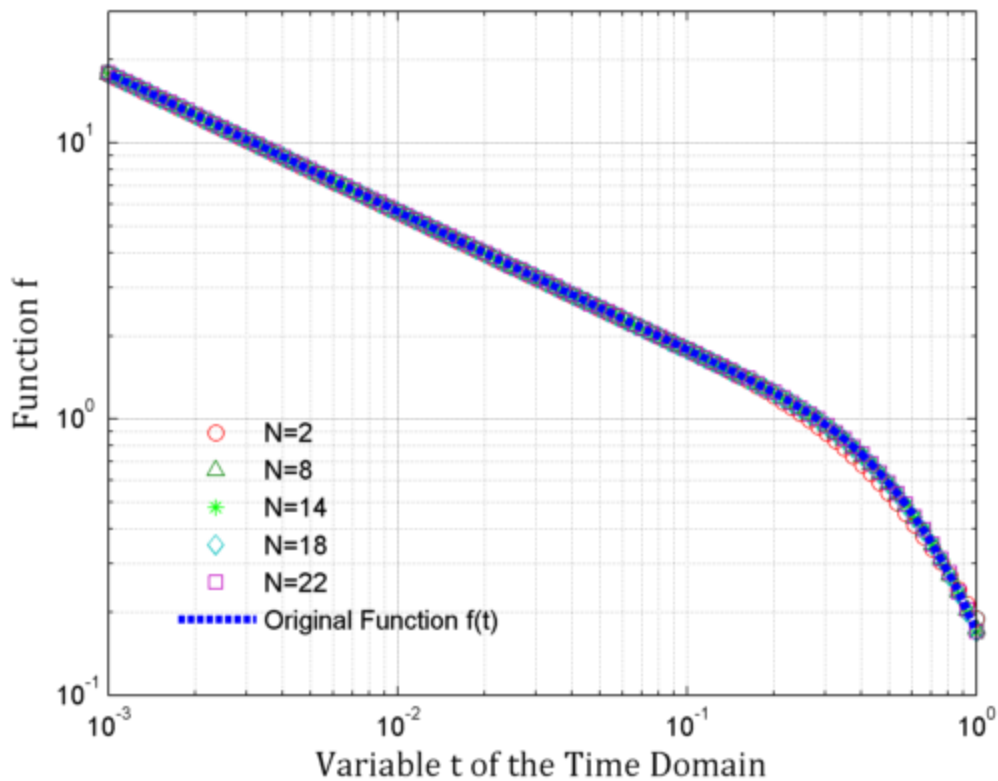
Figure 24:   Original test function compared to the numerical inversion of   computed for several values of time.

Since the numerically inverted solutions calculated for various values of N give good fits to the original function, we can conclude that the Gaver-Stehfest algorithm is valid for the single compartment model. The double compartment model is an extension of the latter: each timescale behaves as a single compartment; therefore we may assume that the Gaver-Stehfest algorithm has the capability to accurately depict the numerical inversion of the Laplace solution of the double compartment model. For each value of N, the time it takes to execute the numerical inversion and the corresponding coefficient of determination, denoted R^2, are recorded and listed in Table 4. For a least number of N,

i.e., $N = 2$, the numerical Laplace inversion is least accurate, however is able to give a fair approximation of the original function. R^2 values are recorded with a precision of ten decimal digits.

N	Time (sec)	R^2
2	0.067	0.9998328680
8	0.179	0.9999999039
14	0.357	1.0000000000
18	0.535	0.9999999999
22	0.732	0.9999687901

Table 4:   Recorded time and R^2 for runs with different values of N

We are able to obtain accurate results with $N = 14$ for our computational machine. Evidently, the more expansion terms in the approximation, the more accurate the approximation is, and the longer it takes to compute. However, increasing of N above 14 yields a lower value of R^2 because N exceeds of the number of decimal digits of precision, i.e., double precision is 16 (Kuhlman 2012).

85

APPENDIX D: A SEMI-ANALYTICAL SOLUTION TO THE RADIAL DIFFUSIVITY EQUATION

In this section, we are going to consider radial flow toward the wellbore. The fundamental theory on this type of flow is composed of the solutions of the equation:

$$\frac{\partial^2 P}{\partial r^2} + \frac{1}{r}\frac{\partial P}{\partial r} = \frac{1}{\alpha}\frac{\partial P}{\partial t} \quad \text{(D.1)}$$

Two sets of solutions of this equation are developed, one for "the constant terminal pressure case" and the other for "the constant terminal rate case" (Everdingen 1949). Each case is then subdivided into either finite or infinite reservoir system. In this appendix, we consider finding an analytical solution to the problem of radial flow with constant terminal pressure in a finite reservoir. But first of all, it is important to present the previously published analytical solution of this radial diffusivity equation. Matthews and Russell (1967) considered a vertical well controlled at a constant bottom hole pressure in a bounded reservoir, and have presented the following solution:

$$
\begin{aligned}
P_D(r_D, t_D) &= \frac{2t_D}{R^2} + \frac{1}{2}\frac{r_D^2}{R^2} - \ln\left(\frac{r_D}{R}\right) - \frac{3}{4} \\
&+ \pi \sum_{n=1}^{n=\infty} \frac{e^{-\alpha_n^2 t_D} J_1(\alpha_n R)[J_1(\alpha_n)Y_0(\alpha_n r_D) - Y_1(\alpha_n)J_0(\alpha_n r_D)]}{\alpha_n[J_1^2(\alpha_n R) - J_1^2(\alpha_n)]}
\end{aligned}
\quad \text{(D.2)}
$$

where J_0, J_1, Y_0, Y_1 are the Bessel functions of the first kind of order zero then one, Bessel functions of the second kind of order zero then one, respectively, and α_n are the roots of the equation:

$$J_1(\alpha_n R)Y_1(\alpha_n) - J_1(\alpha_n)Y_1(\alpha_n R) = 0 \quad \text{(D.3)}$$

As we can see, the well-known analytical solution of the radial diffusivity equation involves functions of roots of more equations, hence is very complicated. To convert this solution into a tool accessible to engineering and applications, it is necessary to resort to numerical approximation. Different flow regimes would employ different assumptions to lead to appropriate mathematical approximations to the solutions. Peters (2012) compiled a comprehensive list of these solutions, among them are pressure solutions at the wellbore for late transient flow and pseudo steady state flow.

In this section considers finding an analytical solution to the problem of radial flow with constant terminal pressure in a finite reservoir. Our ideal system also consists of a single vertical well located at the center of that cylindrical, homogeneous an isotropic reservoir. The radial diffusivity equation to be solved is given by:

$$\frac{\partial^2 P}{\partial r^2} + \frac{1}{r}\frac{\partial P}{\partial r} = \frac{\phi \mu c_t}{k}\frac{\partial P}{\partial t} \qquad \text{(D.4)}$$

A second-order partial differential equation is typically defined by an initial condition and two boundary conditions. We specify that pressure is initially uniform throughout the whole reservoir. Such initial condition is described by the equation:

$$P(r,0) = P_i \qquad \text{(D.5)}$$

We then require the boundary conditions for the internal boundary as well as the external boundary. In our particular problem, we specify constant bottom hole pressure as the internal boundary. This gives rise to the following Dirichlet boundary condition:

$$P = P_{wf} \text{ at } r = r_w \qquad \text{(D.6)}$$

As we can see, Equation (D.6) applies to a well with a finite wellbore radius.

For our bounded reservoir, there is no flow across the external boundary. This gives rise to the following Neumann boundary condition:

$$\frac{\partial P}{\partial r} = 0 \text{ at } r = r_e \qquad \text{(D.7)}$$

The full analytical solution of the above initial-boundary value problem is also the solution to the radial diffusivity equation for the late transient flow period followed by the pseudo steady state flow period. If the dimensionless variables are defined as follows:

$$\begin{cases} P_D = \dfrac{P_i - P}{P_i - P_{wf}} \\[2mm] r_D = \dfrac{r}{r_w} \\[2mm] R = \dfrac{r_e}{r_w} \\[2mm] t_D = \dfrac{k}{\phi \mu c_t r_w^2} t \end{cases} \qquad \text{(D.8)}$$

then the dimensionless form of the initial-value problem becomes:

$$\begin{cases} \dfrac{\partial^2 P_D}{\partial r_D^2} + \dfrac{1}{r_D} \dfrac{\partial P_D}{\partial r_D} = \dfrac{\partial P_D}{\partial t_D} \\[2mm] P_D(r_D, 0) = 0 \\[2mm] P_D(1, t_D) = 1 \\[2mm] \dfrac{\partial P_D}{\partial r_D}(R, t_D) = 0 \end{cases} \qquad \text{(D.9)}$$

Using Laplace Transform as method of solving the partial differential equation, the dimensionless pressure solution in Laplace domain is given by:

$$\hat{P}_D(r_D, s_D) = \frac{1}{s_D} \frac{I_0\left(r_D\sqrt{s_D}\right)K_1\left(R\sqrt{s_D}\right) + K_0\left(r_D\sqrt{s_D}\right)I_1\left(R\sqrt{s_D}\right)}{I_0\left(\sqrt{s_D}\right)K_1\left(R\sqrt{s}\right) + K_0\left(\sqrt{s_D}\right)I_1\left(R\sqrt{s_D}\right)} \qquad \text{(D.10)}$$

where s_D is the dimensionless Laplace variable and is related to s by the relation:

$s_D = \dfrac{\phi\mu c_t r_w^{\,2}}{k}s$ .We then obtain the dimensionless volumetric rate solution in the Laplace

domain by evaluating the first-order spatial derivative of the Laplace pressure at the

wellbore, i.e., $\left.\dfrac{\partial\hat{P}_D}{\partial r_D}\right|_{r_D=1}$:

$$\hat{q}_D(s_D) = \frac{1}{\sqrt{s_D}} \frac{I_1\left(R\sqrt{s_D}\right)K_1\left(\sqrt{s_D}\right) - K_1\left(R\sqrt{s_D}\right)I_1\left(\sqrt{s_D}\right)}{I_0\left(\sqrt{s_D}\right)K_1\left(R\sqrt{s_D}\right) + K_0\left(\sqrt{s_D}\right)I_1\left(R\sqrt{s_D}\right)} \qquad \text{(D.11)}$$

Appendix B presents the numerical approximation of the modified Bessel functions. We will approximate the modified Bessel functions in Equation (D.11) with their lower limits The Bessel functions' limit as the Laplace variable goes to zero corresponds to their late time behavior. An approximation to the dimensionless volumetric rate is thus given by:

$$\hat{q}_D(s_D) = \frac{R^2 - 1}{2 + s_D R^2\left(\dfrac{1}{2}\ln\left[\dfrac{4}{s_D}\right] - \gamma\right)} \qquad \text{(D.12)}$$

Figure 25 depicts the comparison between the exact Laplace solution, Equation (D.11), and its approximation, Equation (D.12), each calculated for several values of R .
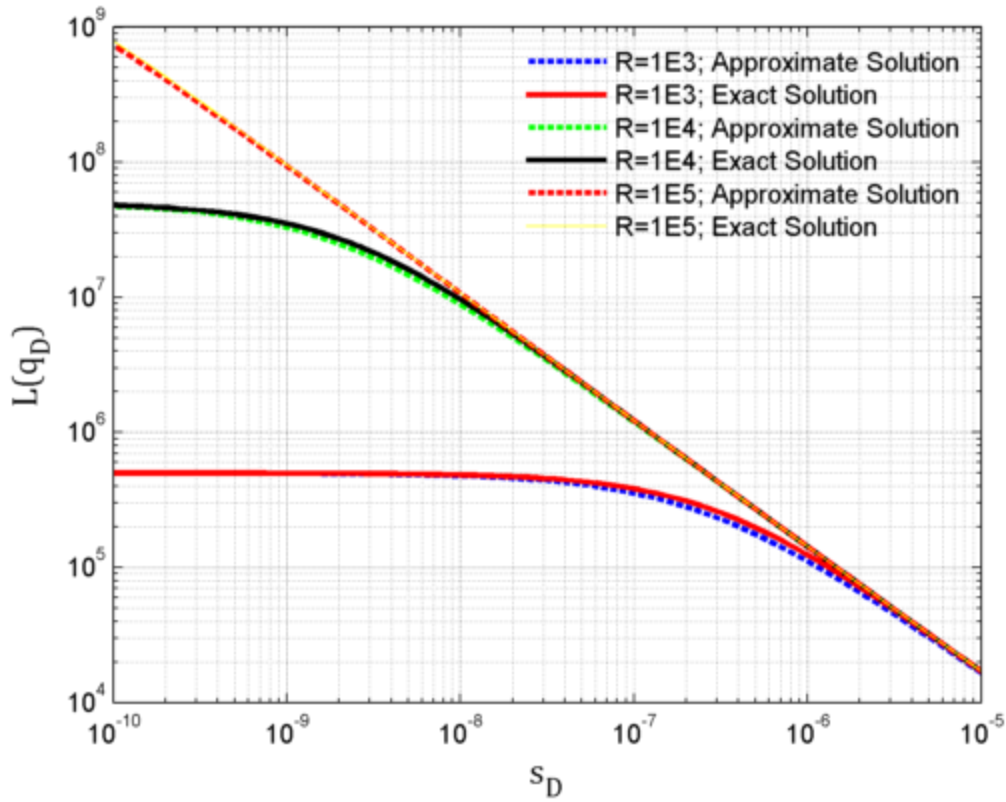
Figure 25:   The exact Laplace solutions compared to its Laplace approximations

Figure shows that the approximate Laplace solution that we intend to use to replace the exact Laplace solution (which involves Bessel functions) is accurate enough with coefficients of determination of $0.9938, 0.9958,$ and 0.9957 for $R = 1E3$, $1E4$ and $1E5$ respectively. However, in order for Equation (D.12) to be useful in our engineering applications, we need to invert it from the Laplace domain back to the time domain.. Next, we employ the Gaver-Stehfest algorithm for numerical inversion of the Laplace Transform, which was introduced in Appendix C, to obtain a closed-form and simple enough solution in the time space. The real-time solution can be written as:

$$q_D(t) = \left[s_D \sum_{n=1}^{N} K_n \hat{q}_D(ns_D) \right]_{s_D = \frac{\ln 2}{t_D}} \quad \text{where } \hat{q}_D(ns_D) = \frac{R^2 - 1}{2 + ns_D R^2 \left(\frac{1}{2} \ln\left[\frac{4}{ns_D} \right] - \gamma \right)} \quad \text{(D.13)}$$

The simplest form, but also the least accurate approximation, can be obtained with the least number of terms, i.e., $N = 2$. Using the Gaver-Stehfest coefficients for $N = 2$ listed in Table 5, one can arrive at the approximated time solution of the dimensionless volumetric rate as:

$$q_D(t_D) = \frac{2(R^2 - 1)\ln(2)}{t_D} \left[\frac{1}{2 + \frac{R^2 \ln(2)}{t_D}\left(\frac{1}{2}\ln\left[\frac{4t_D}{\ln(2)}\right] - \gamma \right)} - \frac{1}{2 + \frac{2R^2 \ln(2)}{t_D}\left(\frac{1}{2}\ln\left[\frac{2t_D}{\ln(2)}\right] - \gamma \right)} \right] \quad \text{(D.14)}$$

Similar expressions but with more expansion terms can be obtained via similar methods. Based on Equation (D.14), the behavior of the dimensionless rate versus the dimensionless time is governed by R, the ratio of reservoir radius to wellbore radius. The dimensional rate, expressed in terms of its non-dimensional form, can be written as:

$$q = \frac{2\ kh(Pi\ \ Pwf)}{}q_D \quad \text{(D.15)}$$

Substituting q_D by (D.14) and t_D by (D.8) into Equation (D.15), we obtain the expression of the approximated volumetric rate at $N = 2$ as:

$$q(t) = \frac{4\ln(2)\pi h \phi \mu c_t (r_e^2 - r_w^2)(Pi - Pwf)}{\mu t} \left[\frac{1}{2 + \frac{\phi \mu c_t r_e^2 \ln(2)}{kt}\left(\frac{1}{2}\ln\left[\frac{4kt}{\phi \mu c_t r_w^2 \ln(2)}\right] - \gamma \right)} - \frac{1}{2 + \frac{2\phi \mu c_t r_e^2 \ln(2)}{kt}\left(\frac{1}{2}\ln\left[\frac{2kt}{\phi \mu c_t r_w^2 \ln(2)}\right] - \gamma \right)} \right] \quad \text{(D.16)}$$

Next, to validate the proposed semi-analytical radial flow model, we reconstruct a vertical well centered in a cylindrical reservoir through numerical simulation then compare the simulation results with the derived equation for the model. The data produces in this work was generated by CMG simulator from Computer Modeling Group Inc. The cylindrical drainage area is divided into eleven concentric cylinder with increasing radius from the block containing the vertical well until the reservoir boundary. The reservoir model parameters are shown in Table 5. The schematics of the reservoir simulation model are shown in Figures 26 and 27.

Reservoir radius	1500 ft
Wellbore radius	0.25 ft
Reservoir thickness	15.2 ft
Initial reservoir pressure	3626 psi
Bottom hole pressure	1450 psi
Porosity	0.065
Permeability	10 md

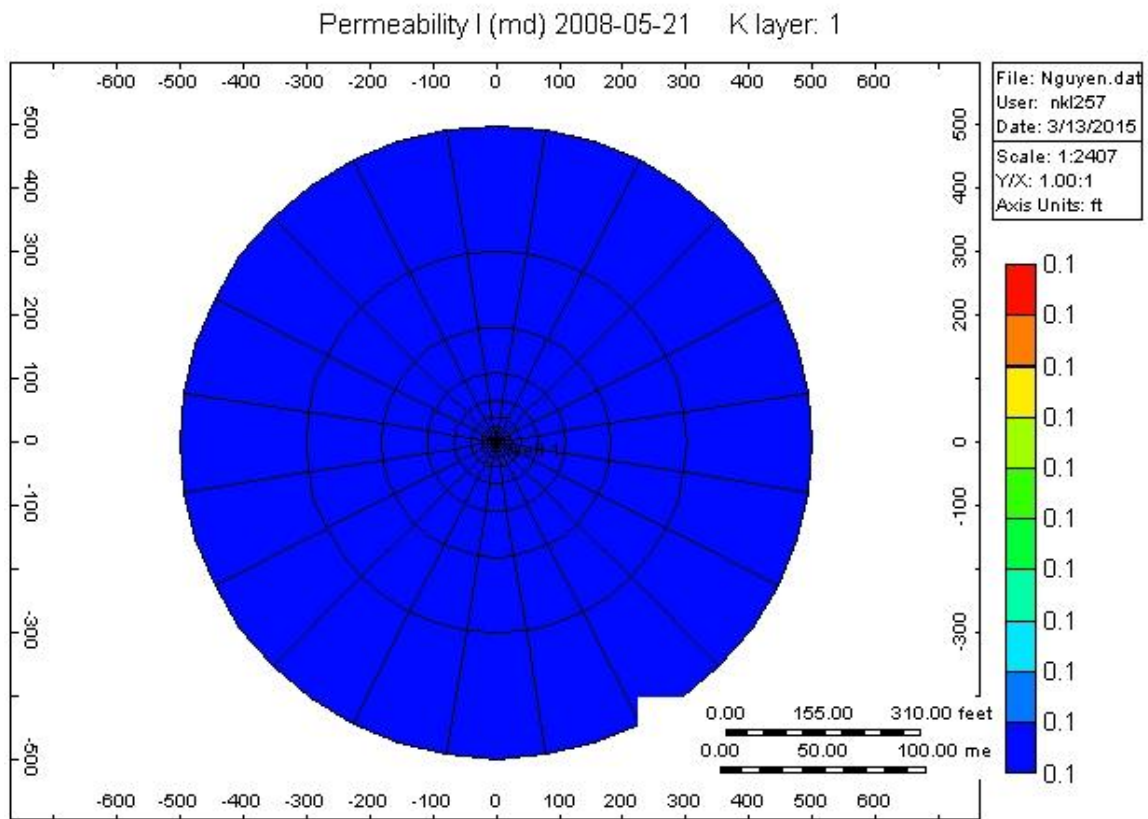Table 5:   Reservoir model specification for the validation of the radial flow model

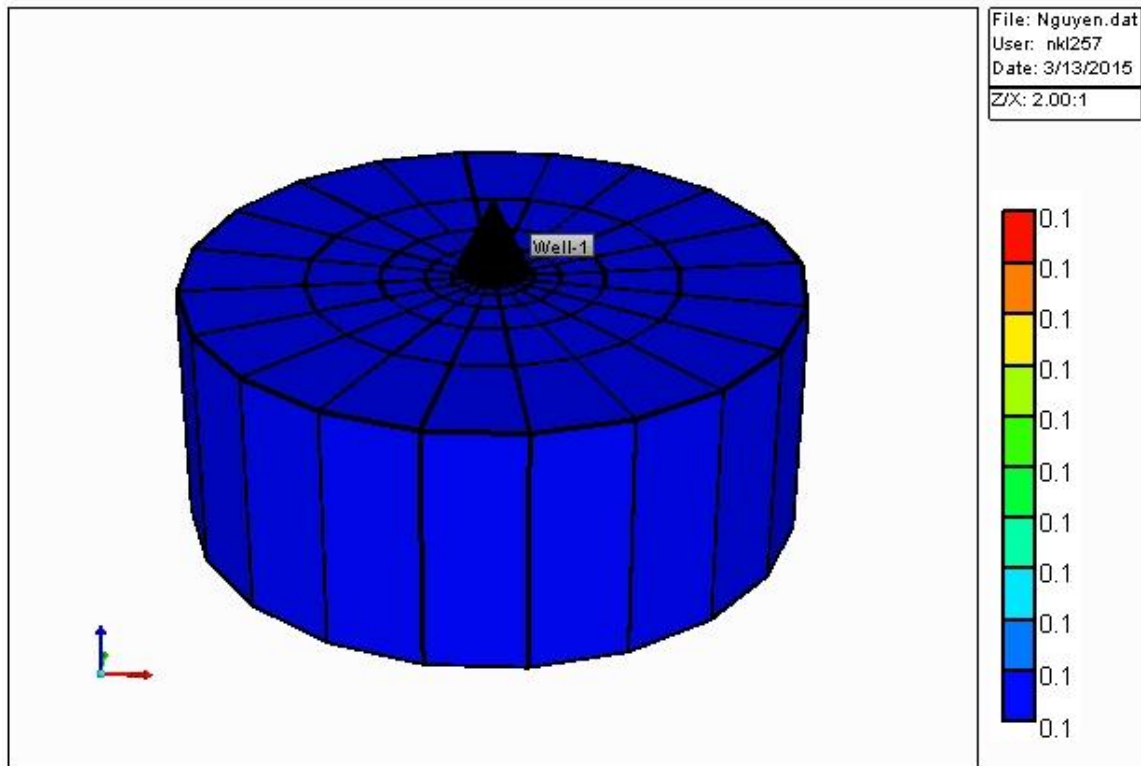Figure 26:   The circular cross section in the z plane of the cylindrical reservoir

Figure 27:   The three-dimensional view of the cylindrical reservoir

Figure 28 depicts the comparison between the simulation results and the semi-analytical models calculated at several values of N
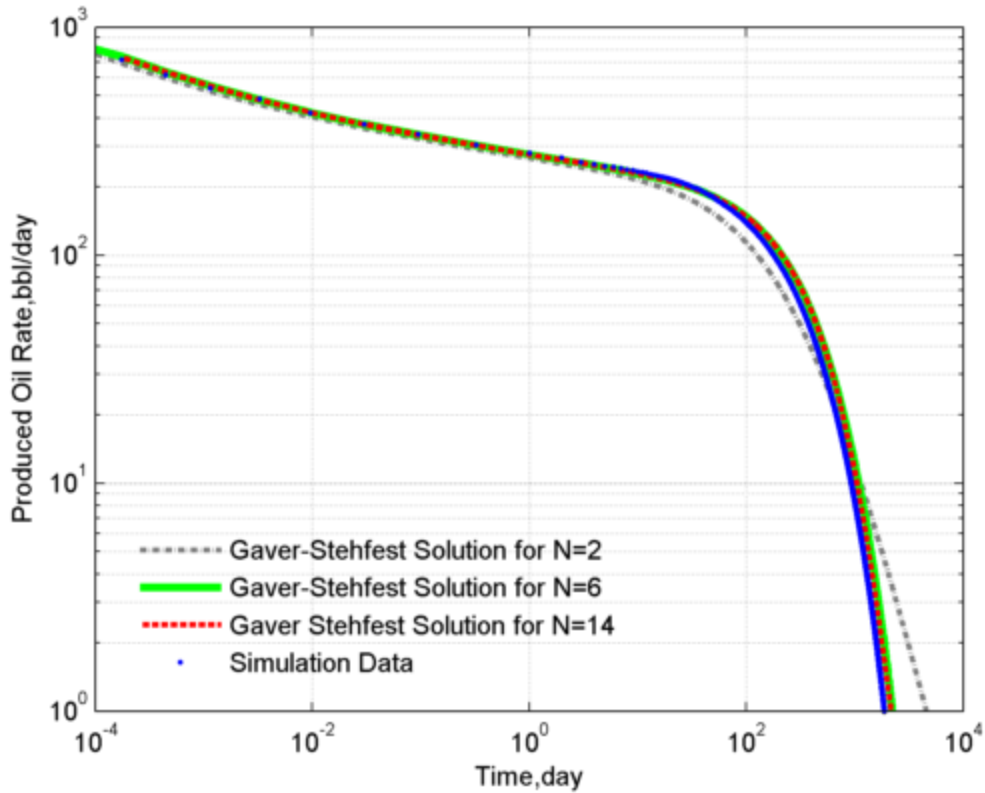
Figure 28:   Comparison between the Gaver-Stehfest solutions calculated at several
             values of time with the simulation results

The simulation results and our model display similar flow characteristics including the radial transient flow regime followed by the pseudo-steady state flow when the effect of the circular reservoir boundary is felt. The Gaver-Stehfest solution calculated for $N=14$ should provide the most accurate approximation possible of the model true solution, whereas that for $N=2$ is the least accurate however offers the form of a semi-analytical solution. Indeed, as shown in Figure 25, the numerical solution computed at $N=14$ proves to fit the simulation data excellently. On the other hand, the semi-analytical solution at $N=2$ does not agree with the part of the simulation data that

corresponds to the reservoir boundary-dominated flow. The lowest value of expansion

terms that provides an acceptable fit is $N = 6$. Depending on the reservoir characteristics,

the number of expansion terms that allows us to obtain an approximation close enough to

the accurate solution varies from case to case.

Nomenclature

y_e : Distance between two parallel fractures

d : Half-distance between two parallel fractures

h : Fracture thickness or pay zone, assuming a fully penetrated fracture

x_f : Fracture half-length

τ_f : Fracture time constant

τ_m : Matrix time constant

ρ : Density

u : Darcy velocity

S_o : Oil saturation

c_o : Oil compressibility

$(c_t)_m$: Matrix total compressibility

ϕ, ϕ_m : Matrix porosity

k_m : Matrix permeability

P_m : Pressure in the matrix

α_m : Matrix diffusivity coefficient

P_i : Initial reservoir pressure

$\bar{P}_f$: Average pressure in the fracture

P_{Dm} : Dimensionless pressure in the matrix

$\hat{P}_{Dm}$: Laplace transform of the dimensionless pressure in the matrix

y_D : Dimensionless distance in the y-direction

t_D : Dimensionless time

t : Time variable

s_D : Dimensionless Laplace variable

s : Laplace variable

A_f : x-y cross sectional area of the fracture

$\hat{q}$: Laplace of the flow rate into one pair of fractures

q : Flow rate into one pair of fractures

q_T : Total flow rate into $N-1$ pairs of fractures

Q_T : Total cumulative produced volume

E : Parameter #1 of the single compartment model

F : Parameter #2 of the single compartment model

EUR : Expected ultimate recovery

L : Distance between two fracture faces

y_f : Thickness of the fracture

P_{wf} : Well flowing pressure

P_f : Pressure in the fracture

P_{Df} : Dimensionless pressure in the fracture

$\hat{P}_{Df}$: Laplace transform of dimensionless pressure in the fracture

x_D : Dimensionless distance in the x-direction

$(c_t)_f$: Fracture total compressibility

ϕ_f : Fracture porosity

k_f : Fracture permeability

α_f : Fracture diffusivity coefficient

ω : Storativity ratio of the fracture and parameter #1 of the dual compartment model

λ : Interporosity flow parameter and parameter #2 of the dual compartment model

q_f : Flow rate into one fracture

q_{fT} : Total flow rate into N fractures

$\hat{q}_f$: Laplace transform of the flow rate into one fracture

$\hat{q}_{fT}$: Laplace transform of the total flow rate into N fractures

A_r : y-z cross sectional area of the fracture

a : Parameter #3 of the dual compartment model

c : Parameter #4 of the dual compartment model

References

Aguilera, R. 1986. An Approximate Solution of Linear Flow in Naturally Fractured Reservoirs. SPE J. SPE-16442.

Archer, R. 2000. Applied Mathematics in Reservoir Engineering. Stanford University. Web. <http://www.stanford.edu/class/energy281/>.

Arps, J. 1945. Analysis of Decline Curves. SPE-945228-G. *Petroleum Transactions*, AIME, 160:228-247.

Bellman, R. and Roth, R. 1984. *The Laplace Transform*. World Scientific Publishing. ISBN: 9971-996-73-5.

Barker, J.A. 1980. Laplace Transform Solutions for Solute in Fissured Aquifers, Water Resour. Res.,1982, Volume 5, 98-104.

Bello, R.O. 2009. Rate Transient Analysis in Shale Gas Reservoirs with Transient Linear Behavior. PhD Dissertation. Texas A&M University, College Station, TX, USA.

Burden, R. and Faires, D. 2011. "Interpolation and Polynomial Approximation." *Numerical Analysis*. Cengage Learning. ISBN: 978-0-53873-351-9.

Chiang, L. 1989. The Application of Numerical Laplace Inversion Methods to Groundwater Flow and Solute Transport Problems. Thesis. New Mexico Institute of Mining and Technology, Socorro, New Mexico, USA.

Furman, A. and Neuman, S. 2003. Laplace-Transform Analytic Element Solution of Transient Flow in Porous Media. Elsevier. Print. 1229-1237.

Guo, B., Lyons, W. and Ghalambor, A. 2007. *Petroleum Production Engineering, A Computer-Assisted Approach*. Gulf Professional Publishing. ISBN: 978-0-75068-270-1.

Hines, K. E., Middendorf, T. R. and Aldrich R. W. 2014. Determination of Parameter Identifiability in Nonlinear Biophysical Models: A Bayesian Approach. Center of Learning and Memory and Department of Neuroscience, The University of Texas at Austin, Austin, TX, USA.

Josso, B. and Larsen, L. 2012. Laplace Transform Numerical Inversion. KAPPA Petroleum Exploration & Production.

Kuchuk, F., Onur, M. and Hollaender, F. 2010. *Pressure Transient Formation and Well Testing- Convolution, Devolution and Nonlinear Estimation*. ISBN: 9780444529534.

Kuhlman, K. L. 2012. Review of Inverse Laplace Transform Algorithms for Laplace-Space Numerical Approaches. Springer Science+ Business Media.

Kuznetsov, A. 2013. On the Convergence of the Gaver-Stehfest Algorithm, Cornell University Library.

Matthews, C.S and Russell, D.G. 1967. Pressure Buildup and Flow Tests in Wells. SPE Monograph Series Vol. 1. ISBN: 978-0-89520-200-0.

Mian, M.A. 1992. *Petroleum Engineering Handbook for the Practicing Engineer, Volume II*. PennWell. ISBN: 0-87814-379-3.

Moench, A. F. and Ogata, A. 1981. A Numerical Inversion of the Laplace Transform Solution to Radial Dispersion in a Porous Medium, Water Resour. Res., Volume 17, Wiley Online Library.

Oberhettinger, F. and Badii, L. 1973. *Tables of Laplace Transforms*. Springer-Verlag. ISBN: 978-3-540-06350-6.

Ogunyomi, B. A., Dong, S., La, N., Lake, L. W. and Kabir, C. S. 2014a. A New Approach to Modeling Production Decline in Unconventional Formations. SPE 170899- MS.

Ogunyomi, B. A., Patzek, T. W., Lake, L. W. and Kabir, C. S. 2014b. History Matching and Rate Forecasting in Unconventional Oil Reservoirs Using an Approximate Analytical Solution to the Double Porosity Model. SPE 171031- MS.

Ogunyomi B. A. 2014c. Mechanistic Modeling of Recovery from Unconventional Oil Reservoirs. PhD Dissertation. The University of Texas at Austin, Austin, TX, USA.

Onur, M. and Reynolds, A.C. 1998. Numerical Laplace Transformation of Sampled Data for Well-Test Analysis. SPE J. SPE-36554-PA.

Peters, E. J. 2012. *Advanced Petrophysics: Volume 1: Geology, Porosity, Absolute Permeability, Heterogeneity, and Geostatistcis*. Live Oak Book Company. ISBN: 978-1-936909-44-5.

Satter, A., Iqbal, G. and Buchwalter, J. 2007. *Practical Enhanced Reservoir Engineering: Assisted With Simulation Software*. PennWell. ISBN: 978-1-59370-056-0.

Stehfest, H. 1970. Numerical Inversion of Laplace Transforms. Communication of the ACM. No.1, 47-49.

Stewart, G. 2011. *Well Test Design & Analysis*. PennWell Corporation. ISBN: 978-1-59370-231-1.

Van Everdingen, A.F. and Hurst, W. 1949. Application of the Laplace Transformation to Flow Problems in Reservoirs. AIME, 186: 305-326.

Walsh, M. P. and Lake, L. W. 2003. *A Generalized Approach to Primary Hydrocarbon Recovery*. Elsevier. ISBN: 978-0-444-50683-2.

Xu, W., Li, J. and Du, M. 2011. Quick Estimate of Initial Production from Stimulated Reservoirs with Complex Hydraulic Fracture Network. SPE J. SPE-146753.